

AN ABSTRACT OF THE THESIS OF

Morgan Messer for the degree of Master of Science in Mechanical Engineering presented on May 9, 2022.

Title: Fouling Characterization in Hypersaline Wastewater Treatment

Abstract approved: _____

Bahman Abbasi

Water supplies are diminishing worldwide and by 2025 two thirds of the population could be living in regions of water scarcity (local demand for water is greater than water supply). One method to increase available water sources is to use desalination technologies to separate water from saline solutions. While desalination itself isn't a new idea the process is being expanded to determine how it can be used to treat other contaminated wastewater sources that otherwise wouldn't be treated which reduces the overall water available. In this aspect a water treatment system is being developed at the Water and Energy Technology Laboratory at Oregon State University to treat hydraulic fracturing wastewater.

The SCEPTER (Selective Condensation and Evaporation using Precise Temperature Regulation) system requires a humidification dehumidification (HDH) process to separate different contaminants from the produced water stream. This thesis is part of the research to develop a humidification system that is reliable, low energy, competitive cost, mitigates fouling, and separates contaminants to produce irrigation level water.

Two different humidification techniques are reviewed: spray humidification, and a venturi nozzle paired with an evaporator humidification system. Spray humidification while 20-30% less energy intensive than venturi nozzle humidification has a much higher risk of recontaminating the produced water as contaminants can become entrained in the humid air stream and would require additional components to remove them. Whereas the venturi nozzle

humidification system is more energy intensive it has a lower risk of contaminating the produced water and is can still be cost competitive with other technologies.

As the evaporation zone has the highest risk of fouling due to the high salinity and salt separation a study was done to understand the fouling resistance over time for a highly saline mixture with various surface roughness'. Reducing the surface roughness is beneficial if it is greatly reduced (0.35 μm) but if it is still sufficiently rough (homogeneous 5 μm or 10.5 μm average roughness with microchannels) there is minimal change to the fouling resistance or heat transfer coefficient during pool boiling with 20% saline concentrated seawater.

Lastly an evaporation zone was designed to test crystallization fouling in a flow boiling environment and to understand how to mitigate fouling effectively. An electrically heated aluminum pan containing baffles to control the flow path was used to test 10% NaCl and 10% KCl saline solutions at different flow rates (2.3-3.1 g/s) to inform system operating parameters. Maintaining water evaporation rates less than 54% stayed free of fouling (scaling) for 4 hours. If the system operated with a higher water evaporation rate a targeted flush was identified as an applicable fouling mitigation method. Targeted flushing was used on areas where fouling accumulated which allowed the overall evaporation rate to remain unchanged and allowed the system to continue to operate without maintenance.

This work can be utilized to estimate the fouling resistance and heat transfer coefficient for a 20% saline mixed salt seawater solution during pool boiling for various surface roughness' and inform heat exchanger surface roughness design and operation. The evaporation zone work can be utilized when designing other evaporation systems and the operational parameters to avoid fouling can be used to reduce fouling accumulation. In addition, targeted flushing can be a method to mitigate fouling if it does occur in a flow boiling system.

©Copyright by Morgan Messer

May 9, 2022

All Rights Reserved

Fouling Characterization in Hypersaline Wastewater Treatment

by
Morgan Messer

A THESIS

submitted to

Oregon State University

in partial fulfillment of
the requirements for the
degree of

Master of Science

Presented May 9, 2022

Commencement June 2022

Master of Science thesis of Morgan Messer presented on May 9, 2022

APPROVED:

Major Professor, representing Mechanical Engineering

Head of the School of Mechanical, Industrial, and Manufacturing Engineering

Dean of the Graduate School

I understand that my thesis will become part of the permanent collection of Oregon State University libraries. My signature below authorizes release of my thesis to any reader upon request.

Morgan Messer, Author

ACKNOWLEDGEMENTS

To my parents, Korby and Suzanne, thank you for always believing in me, pushing me to do my best, and all of your guidance throughout the years. You reminded me (constantly) growing up that hard work was good for me and that I could do whatever I put my mind to. To my siblings who inspire me with their own achievements and make me want to do better. I can't wait to see what you all achieve.

To my advisor Dr. Abbasi for your support and mentorship both in this degree and during my undergraduate degree. I am incredibly grateful to you for reaching out during my undergraduate degree and pushing me to pursue a master's degree. You pushed me to grow and learn new things which helped me grow as a researcher, presenter, and engineer these last few years.

To Brayden I am so grateful for your unwavering support and encouragement which allowed me to pursue this degree and helped motivate me. You were always there to help me sort through problems and put up with listening to my daily updates/ramblings on my work and classes. You've always had confidence in me even when I wasn't confident in myself.

To my friends you are the best support I could have asked for! I am so grateful to have so many friends who have supported me in this degree and put up with my crazy schedule. I will miss working with everyone at the WET lab. You made the days bearable when nothing made sense, and everything went wrong during experiments. To our occasional Friday lunches that helped keep me sane during this degree.

Thank you all!!!

TABLE OF CONTENTS

	<u>Page</u>
CHAPTER 1: Introduction	1
1.1. Water shortages and desalination background.....	1
1.2. Fracking wastewater background.....	1
1.3. Fouling background	2
1.4. SCEPTER	2
1.5. Thesis objectives.....	3
1.6. Thesis organization	4
References.....	6
CHAPTER 2: Comparative analysis of humidification techniques.....	8
Abstract.....	9
2.1. Introduction.....	9
2.1.1. Our HDH process.....	10
2.1.2. Direct contact condenser	11
2.1.3. Humidification techniques	12
2.1.3.1. Spray humidification.....	12
2.1.3.2. Venturi nozzle humidification	13
2.2. Energy consumption	13
2.2.1. Energy comparison	14
2.3. Contaminant separation	15
2.3.1. Salt management.....	16
2.3.1.1. Spray humidification - Salt management.....	16
2.3.1.2. Venturi nozzle humidification - Salt management.....	16

TABLE OF CONTENTS (Continued)

	<u>Page</u>
2.3.2. Azeotropes	17
2.4. System complexity	17
2.5. Conclusions.....	18
References.....	18
CHAPTER 3: Surface roughness fouling with mixed salts	20
Abstract.....	21
3.1. Introduction.....	21
3.1.1. Salt concentration and types	22
3.1.2. Surface roughness effect on fouling.....	23
3.1.3. Boiling effect on fouling	24
3.1.4. Ethylene glycol effect on fouling.....	25
3.1.5. Current work	25
3.2. Experimental setup.....	26
3.3. Methodology	30
3.3.1. Simulation results.....	32
3.3.2. Uncertainty propagation.....	33
3.4. Results and discussion	34
3.4.1. Temperature difference	34
3.4.2. Effect of surface roughness on fouling	35
3.4.3. Effect of ethylene glycol on fouling	37
3.4.4. Effect ethylene glycol on salt composition	41
3.5. Conclusion	42
Nomenclature.....	44

TABLE OF CONTENTS (Continued)

	<u>Page</u>
References.....	45
CHAPTER 4: Crystallization fouling management in hypersaline flow boiling	48
Abstract.....	49
4.1. Introduction.....	49
4.1.1. Boiling.....	50
4.1.2. Flushing.....	51
4.1.3. System design	51
4.1.4. This study.....	52
4.2. Experimental setup.....	52
4.3. Methodology	54
4.3.1. Uncertainty analysis.....	56
4.4. Oversaturation location model to inform fouling mitigation strategies	56
4.5. Results and discussion	59
4.5.1. Evaporation rate and cost of produced water.....	59
4.5.2. Fouling	62
4.5.3. Flushing.....	63
4.6. Conclusion	64
References.....	66
CHAPTER 5: Thesis conclusions and future recommendations	68
5.1. Thesis summary	68
5.2. Future recommendations.....	69

LIST OF FIGURES

<u>Figure</u>	<u>Page</u>
Figure 1.1 Process schematic of a single module of SCEPTER.....	3
Figure 2.1 OSU's oil and gas wastewater purification system.....	11
Figure 2.2 Schematic and CAD of the direct contact condenser.....	12
Figure 2.3 Experimental setup for spray humidification: a) simplified schematic b) experimental setup.....	14
Figure 3.1. Experimental setup used to determine the fouling resistance and the heat transfer coefficient for various surface roughness and solutions A) experimental schematic, B) schematic showing the top view of the aluminum block, C) actual setup.....	28
Figure 3.2. Aluminum block with different roughness, 0.35 μm and 5 μm were achieved using sandpaper creating a homogeneous surface roughness, and 10.5 μm was achieved with a Dremel creating microchannels and a heterogeneous surface.....	28
Figure 3.3. SOLIDWORKS simulation showing radial temperature distribution for $q''=66,000 \text{ W/m}^2$ and 97.4°C water temperature. 2-4% error compared to measured thermocouple data.....	33
Figure 3.4. Impact of surface roughness on fouling resistance.....	35
Figure 3.5A. Impact of surface roughness on fouling resistance.....	37
Figure 3.5B. Impact of surface roughness on heat transfer coefficient.....	37
Figure 3.6A. Impact of surface roughness and ethylene glycol (EG) on fouling resistance...	39
Figure 3.6B. Impact of surface roughness and ethylene glycol (EG) on heat transfer coefficient.....	40
Figure 3.7. Example pictures of crystallization fouling for 0.35 μm , 5 μm , 10.5 μm , and 10.5 μm with 3% ethylene glycol in the solution after 140 minutes.....	40
Figure 3.8. ICP-OES data showing the elements that accumulated on the aluminum block's surface for a 10.5 μm surface roughness with (Salt 2) and without (Salt 1) 3% ethylene glycol present in the solution.....	42

LIST OF FIGURES (Continued)

	<u>Page</u>
Figure 4.1 Experimental setup of a bottom heated evaporation system A) full experimental setup, B) close up of the evaporation pan and the flush inlet location, C) experimental setup with a polycarbonate lid, D) CAD diagram of evaporation pan showcasing the 4 heater's positions. (1) preheated mixed solution, (2) Masterflex L/S displacement pump, (3) Aluminum evaporation pan, (4) Belee 20 A variable voltage transformer Baldr power meter, (5) DIPump550 displacement pump, (6) discharge container, (7) Dymo M10 scale, (8) polycarbonate lid with vapor outlet.....	54
Figure 4.2: Boiling and fouling locations of experiment and code estimates for 2.8 g/s 10% NaCL and 10% KCl saline.....	58
Figure 4.3: Fouling location at A) 11, B) 13, C) 15, D) 19, and E) 24 minutes during a 2.3 g/s inlet flow rate test	63
Figure 4.4: Pictures before (left) and after (right) of the aluminum pan fouling after a 24 second flush at 4.6 g/s.....	64

LIST OF TABLES

<u>Table</u>	<u>Page</u>
Table 2.1. Experimental data for spray humidification.....	15
Table 3.1. Salts used in a representative seawater composition	29
Table 3.2. Testing solution for experiments with and without Ethylene glycol.....	29
Table 3.3. Surface roughness crystallization fouling experimental test matrix.....	30
Figure 3.4. Impact of surface roughness on fouling resistance.....	34
Table 4.1. Uncertainty in parameters for tests performed on the evaporation system...	56
Table 4.2. Evaporation and cost of produced water results for various 20% saline water flow rates (2.3-3.1 g/s)	61

DEDICATION

*For my parents, Mrs. Suzanne Messer and Mr. Korby Messer, my
siblings, Victoria, Piper, and Zane, and for Brayden*

CHAPTER 1: Introduction

1.1. Water shortages and desalination background

Water supplies are diminishing worldwide causing droughts in many countries as the demand for water increases and water sources are not replenished (referred to as water scarcity). Over 2.3 billion people experience water stress at least one month a year and by 2025 two thirds of the population could be living in water scarcity regions [1], [2].

With the amount of available freshwater diminishing and contaminated water sources rising, there are more technologies under development aimed at treating less ideal water sources to improve water supplies. These water sources include brackish water, highly saline (brine) wastewater, industrial/municipal wastewater, and hydraulic fracturing wastewater etc.

Desalination is one water treatment method that can be used to treat water by separating salts and minerals to produce water. This method is commonly utilized to treat seawater (1-3.5% saline water) [2].

Desalination is classified by the method of separation: thermal or membrane based. Where thermal desalination separates salts via evaporation and condensation and membrane desalination allows water to diffuse through a membrane trapping the salts to one side. There are many different types of desalination methods that are utilized worldwide producing water for over 300 million people in 150 countries [3].

1.2. Fracking wastewater background

While treating both seawater and other lightly contaminated water using desalination is extremely helpful to ensuring increased water supplies; many technologies are focusing on treating highly contaminated wastewater, such as hydraulic fracturing wastewater, that is otherwise left untreated and if not contained could contaminate freshwater sources. Hydraulic fracturing utilizes 8,000 – 80,000 m³ of water per well (in 2014 977,000 hydraulic fracturing wells were consuming and contaminating water) the majority of which is disposed of in injection wells where the water is contained but unusable [4], [5]. With an increase in hydraulic fracturing to produce oil and gas there is an equal increase in wastewater produced from the process. Available injection well space has not increased which has led to concerns about the sustainability of the process and concerns about contaminating clean water

resources. Treating hydraulic fracturing wastewater is very difficult as different wells have different contaminants and concentrations and each company can add proprietary chemicals to the water before use to improve oil and gas extraction [6]. Furthermore, hydraulic fracturing wastewater is difficult to treat as it is highly saline and even at lower salinities desalination treatment plants have a difficult time managing fouling.

1.3. Fouling background

Fouling or unwanted surface material deposits are problematic in water treatment and desalination systems and heat exchangers. Fouling causes lower heat transfer efficiency, increased pressure drops, increased corrosion, reduced flow, blockages, corrosion etc., which can increase maintenance cost and reduce operation time. Fouling can be classified as biological, corrosion, particulate, chemical, or crystallization fouling (scale, inorganic fouling, precipitation fouling) [7]. In 2000, fouling cost the US \$8,000-\$10,000 million most of which was from crystallization fouling [8]. Crystallization fouling occurs when salts separate from the mixture and adhere to a surface where they become difficult to remove. Over 70% of fouling in desalination systems is crystallization fouling as seawater is mostly inorganic [9]. The crystallization fouling is dependent on the degree of salt saturation, types of salts, number of salts present, operational parameters (velocity, temperatures, orientation), nucleation sites etc. which all make it difficult to predict and control [10].

Various methods to mitigate fouling have been utilized and studied. These methods include adding chemicals to the solution to target specific foulants, increasing flow velocity and reducing stagnation, adjusting the surface roughness, adding a surface coating, utilizing vibrations or ultrasonic, or a physical device (beads, cleaning sponges, secondary setup, rotating parts) to reduce and remove fouling [11]. Multiple fouling mitigation techniques are used as one single technique is generally not enough to completely mitigate fouling.

1.4. SCEPTER

SCEPTER (Selective Condensation and Evaporation using Precise Temperature Regulation) (Patent Application Number: 62882970) provides a solution to treat highly contaminated hydraulic fracturing wastewater [12]. As shown in Figure 1.1, wastewater is fed into a settling tank where it is preheated using a heat exchanger. The contaminants are separated via gravity at the bottom of the settling tank and the lighter density components (ex. oils) rise to the top of the settling tank where they can be easily removed. The wastewater is pumped from the settling tank to an evaporation zone where the solution is partially evaporated which manages

fouling and separates the contaminants with higher boiling points than water. The unevaporated mixture is fed back to the settling tank where the salts can precipitate and be removed. The steam and more volatile contaminants making up the evaporated mixture are mixed with a preheated air stream before moving to a direct contact condenser (DCC) where the steam is condensed with a cooling water flow and separated from the more volatile contaminants. The volatile contaminants exit with the air stream at the top of the condenser. The cooling water can be recirculated and separated from the produced water. The produced water contains less than 1% contaminants by mass allowing it to be usable for industrial reuse and with further development even for irrigation [13].

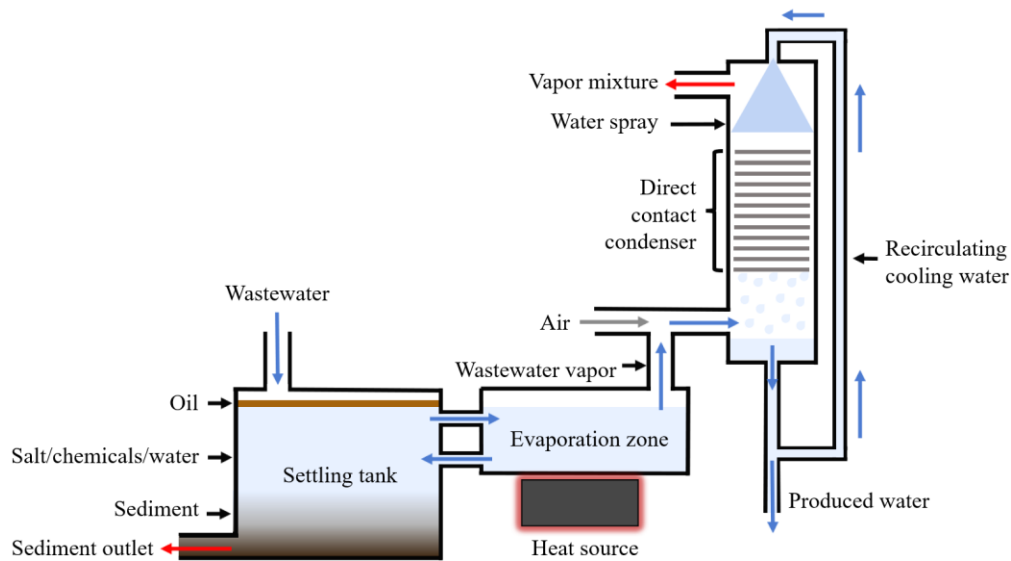


Figure 1.1 Process schematic of a single module of SCEPTER

1.5. Thesis objectives

Different humidification methods were reviewed as potential options to humidify the wastewater stream and separate less volatile contaminants and dissolved solids. Humidifying the wastewater stream is the most energy intensive part of the SCEPTER system and is the most likely to encounter high fouling as it has the highest contaminants and reduces the water available for them to stay dissolved. If not managed, the fouling reduces system efficiency and inhibits the system from operating correctly. The humidification system needed to be robust to handle a wide range of contaminants and concentrations while managing the energy input to ensure the system is cost competitive with other purification technologies. This outlines the following research questions:

- A comparison between spray evaporation and flow evaporation is needed to assess the energy input and water quality to determine their compatibility with SCEPTER.
- Fouling accumulation must be quantified to identify the impact of surface roughness on fouling.
- Crystallization fouling must be characterized and managed during flow boiling.

As fouling is difficult to predict and few studies have been done to characterize fouling accumulation and its effects in highly saline (20%) mixed salt pool boiling applications with various surface roughness' it became necessary to test. As fouling has a large impact on heat transfer performance it is important to understand how long it takes for the fouling to accumulate and the effect on the overall system performance to design for a steady state operational point. The study also included experiments to understand how adding ethylene glycol (a common compound in hydraulic fracturing wastewater) would affect the fouling accumulation and the fouling composition.

An evaporation zone was built and tested to understand how operating procedures could be utilized to reduce fouling in a system such as SCEPTER. As SCEPTER is designed to operate at salinities close to and at salt saturation understanding and identifying an acceptable evaporation rate while controlling the fouling was imperative for providing targets for the control system to operate between. This work ensures that the system can be operated for several hours and controlled by changing the inlet flow rate while monitoring the evaporation rate. This is important for near-continuous operation and to maximize water production by minimizing downtime and flushing. Lastly targeted flushing, a fouling mitigation technique, was demonstrated in the evaporation zone to mitigate fouling when it did occur and ensure minimal disruption to the system.

1.6. Thesis organization

Chapter 2, two humidification methods are compared to determine their applicability in SCEPTER, a new humidification-dehumidification (HDH) system designed to treat oil and gas wastewater. A spray humidification technique using a patented anticlogging atomizer and a venturi mixing nozzle paired with a surface boiling system were compared in an experimental and analytical study to determine the impact of each method on the overall process operation and energy consumption [14]. Spray humidification consumed 20-30% less energy per unit of water but had a risk of entraining dissolved solids in the humid stream, whereas venturi mixing nozzle humidification was more energy intensive but had minimal to

no risk of recontamination. This chapter presents experimental data, analysis, and provides a comparison of the two humidifiers and their effect on energy and operation of an HDH wastewater treatment system. This work resulted in a peer-reviewed conference paper for the International Desalination Association (IDA) 2021 International Water Reuse and Recycling Conference in Rome, Italy in 2021.

Chapter 3 presents a study showing the effect of surface roughness on mixed salt crystallization in high salinity (20%) pool boiling environment. Experiments were performed to determine the effect of changing the heat exchanger's surface roughness between an average roughness of 0.35 μm , 5 μm , and a microchannel surface with average roughness (channel size) of 10.5 μm on the heat transfer coefficient, fouling resistance, and salt composition. The 0.35 μm surface had 1.5 $\text{cm}^2\text{K/W}$ less fouling resistance than the homogeneous 5 μm and microchannel 10.5 μm surfaces that had nearly identical fouling resistances (2.7 $\text{cm}^2\text{K/W}$). Decreasing the surface roughness is only beneficial if it is sufficiently reduced but if it is still sufficiently rough (homogeneous 5 μm - 10.5 μm microchannel average roughness) there is no impact on fouling accumulation. In addition, tests were performed to quantify the effect of adding 3% ethylene glycol to the saline mixture. It had minimal impact on the fouling accumulation but did change the composition of the salts that adhered to the surface. This work resulted in a manuscript for the Journal of Heat transfer (submitted – under peer review)

Chapter 4 presents a study focused on mitigating crystallization fouling in a 20% saline (10% NaCl and 10% KCl) flow boiling environment. An electrically heated aluminum pan with baffles, to control the flow path and residence time, was designed to determine the conditions where fouling could be managed. The flow rate was varied from 2.3-3.1 g/s with 3,730 W of electrical heating input and found for flow rates 2.9-3.1 g/s no fouling occurred in the system after 4 continuous hours of steady state operation with a water evaporation rate of 52-54%. Whereas, at lower flow rates fouling began to accumulate in the first 30 minutes of testing and would require a fouling mitigation method to reach steady state operation, such as a water flush. By targeting the specific areas where fouling occurred in the system by flushing that area with water, fouling could be removed and managed without impacting the evaporation rate. This work resulted in a manuscript which will soon be submitted.

Chapter 5 presents a summary of the thesis outlining the technical and scientific developments. Potential applications of this work include an understanding of how different

humidification techniques can be utilized to treat highly contaminated saline wastewater, improved predictions for highly saline seawater, or mixed salt, fouling in a boiling environment, improved understanding of operating parameters to reduce crystallization fouling, and an example of how to apply water flushing to mitigate fouling. Areas for future work are also presented.

Nomenclature (if required by the publisher), author contributions, and literature sources are provided individually at the end of each chapter.

References

- [1] United Nations, "Summary Progress Update 2021: SDG 6 — water and sanitation for all," 24 February 2021. [\[Online\]](#).
- [2] F. Macedonio, E. Drioli, A. A. Gusev, A. Bardow, R. Semiat and M. Kurihara, "Efficient technologies for worldwide clean water supply," *Chemical Engineering and Processing*, vol. 51, pp. 2-17, 2012.
- [3] Aqua Tech, "Desalination: Our Essential Guide To Desalination and the Global Water Crisis," 2 October 2019. [\[Online\]](#).
- [4] R. B. Jackson, A. Vengosh, J. W. Carey, R. J. Davies, T. H. Darrah, F. O'Sullivan and G. Pétron, "The Environmental Costs and Benefits of Fracking," *Annual Revision Environment Resources*, vol. 39, pp. 327-362, 2014.
- [5] T. Cook, J. Perrin and D. V. Wagener, "Hydraulically fractured horizontal wells account for most new oil and natural gas wells," *EIA*, 30 January 2018. [\[Online\]](#).
- [6] H. O'Hern, E. Nikooei, X. Zhang, C. Hagen, N. AuYeung, D. Tew and B. Abbasi, "Reducing the water intensity of hydraulic fracturing: a review of treatment technologies," *Desalination Water Treatment*, vol. 221, pp. 121-138, 2021.
- [7] Brazetek Heat Exchangers, "Mechanisms of fouling," 2012. [\[Online\]](#)
- [8] J. MacAdam and S. A. Parsons, "Calcium carbonate scale formation and control," *Reviews in Environmental Science and Bio. Technology*, vol. 3, pp. 159-169, 2004.
- [9] D. Rubio, C. López-Galindo, J. F. Casanueva and E. Nebot, "Monitoring and assessment of an industrial antifouling treatment. Seasonal effects and influence of water velocity in an open once-through seawater cooling system," *Applied Thermal Engineering*, vol. 67, no. 1-2, pp. 378-387, 2014.
- [10] M. Messer, K. Anderson, X. Zhang and B. Abbasi, "Effect of Surface Roughness on Mixed Salt Crystallization Fouling in Pool Boiling," *Journal of Heat Transfer*, 2022 (submitted – under peer review).
- [11] M. Bagheri and S. A. Mirbagheri, "Critical review of fouling mitigation strategies in membrane bioreactors treating water and wastewater," *Bioresource Technology*, vol. 258, pp. 318-324, 2018.
- [12] B. Abbasi, X. Zhang, H. O'Hern and E. Nikooei, "Method and System for Purifying Contaminated Water". United States Patent 62882970, 4 August 2020.

- [13] E. Nikooei, N. AuYeung, X. Zhang, K. Goulas and B. Abbasi, "Controlled dehumidification to extract clean water from a multicomponent gaseous mixture of organic contaminants," *Journal of Water Process Engineering*, vol. 43, 2021.
- [14] B. Abbasi, X. Zhang, M. A. Elhashimi Khalifa and D. Sharma, "Method and apparatus for desalinating water". US Patent 20210039008A1, 11 February 2021.

CHAPTER 2: Comparative analysis of humidification techniques

Morgan Messer¹, Xiang Zhang¹, Xu Tan², Mohammed A. Elhashimi¹, André Bénard²,
Bahman Abbasi^{1*}

Oregon State University, Corvallis, OR 97331, USA

Oregon State University-Cascades, Bend, OR 97702, USA

*Corresponding author: AbbasiB@oregonstate.edu

International Desalination Association (IDA) 2021 International Water Reuse and Recycling
Conference

Rome, Italy 2021

An Experimental and Comparative Analysis of Humidification Techniques for Oil and Gas Wastewater Treatment

Abstract

The authors have developed and published a new humidification-dehumidification (HDH) method to treat oil and gas wastewater. The process humidifies air with water containing volatile contaminants while leaving dissolved solids and heavy organics behind. In a later stage, water is selectively condensed to obtain clean water. By separating the solids upfront, the process eliminates fouling in most of the system. The humidifier is the most energy-intensive component of the HDH unit, and its design impacts the overall operation of the system. This article presents the findings from an experimental and analytical study on the effects of humidification techniques on the process operation and energy consumption. Two humidifiers are assessed: a spray humidification technique using our patented anti-clogging atomizer and a venturi mixing nozzle paired with a surface boiling system. As expected, spray humidification consumed 20-30% less energy per unit of water by operating at lower temperatures. However, precise control of spray evaporation is needed to avoid precipitating dissolved solids which can be entrained in the humid air stream, foul the dehumidification system, dissolve in condensed water, and cause recontaminate. Mixing nozzle humidification relies on surface boiling, which is more energy intensive, but it poses no risk of entraining solids in the humid stream and fouling the condenser or recontaminating the clean water. This paper presents the experimental data, analyses, and provides a detailed comparison of these two humidifiers and how they affect the operation of an HDH wastewater treatment system. The findings help guide future HDH process design.

Keywords: Spray humidification, Nozzle humidification, Wastewater treatment

2.1. Introduction

The advancement of unconventional oil and gas production techniques has increased energy security in the United States and around the world. The process involves injection of high-pressure fluid into shale rock to mine oil and natural gas that otherwise is too expensive to

mine. However, the expansion of unconventional oil and gas production has caused concerns regarding the large volume of toxic wastewater produced. Approximately 7.5 million cubic meters of oil and gas wastewater are stored in deep injection wells per day in the United States [1]. Additionally, most existing water purification technologies are not compatible with process oil and gas wastewater, as no qualitative nor quantitative data are available for the composition of contaminants. O'Hern et al. [2] presented a discussion on the advantages and drawbacks of different water purification options for hydraulic fracturing wastewater treatment. One promising method for wastewater is to use a humidification-dehumidification (HDH) process to separate contaminants such as salts, oils, volatile organics, acids, etc. HDH systems are thermally driven and less expensive to couple with a renewable power source, such as solar energy, compared to other water purification techniques [3].

In this regard, a humidification-dehumidification based oil and gas wastewater purification system is under development at Oregon State University (OSU) to produce clean water for irrigation purposes. The system needs to separate various contaminants with various concentrations as different oil and gas companies add different chemicals to the water. Furthermore, each oil and gas wastewater production location may collect different compounds and concentrations specific to that location's geological composition. The system uses low energy input to reduce fouling of the components within the system and maximize the cleaned water production to be reused elsewhere. There are many ways to humidify air. When choosing a humidification process the primary elements to consider are overall complexity, fouling potential, cost, energy input, and process compatibility. Commonly used packed bed humidifiers are not ideal for use with wastewater as the high concentration of contaminants in the wastewater will foul the packed bed quickly and require frequent cleaning and replacing of the packed bed. Zubair et al. [9] investigated a humidification system that utilized a packed bed to purify saline water with seawater salinity; it required cleaning every 2 weeks and a replacement packed bed every 2 months. This paper compares a spray humidification and a venturi nozzle humidification design as these are common desalination techniques that have great potential with highly contaminated water.

2.1.1. Our HDH process

In our patented-pending oil and gas wastewater purification system (shown in Figure 2.1), the wastewater enters the system (1) and flows through a heat exchanger to be preheated (2). The water then flows into a settling tank, ensuring the contaminated mixture is consistent and free

of any suspended compounds (3) before entering the humidification system (4). Either spray or venturi nozzle humidification is used to humidify a carrier air stream [4]. The humid air flows to the direct contact condenser (DCC) (5) to be dehumidified. The DCC condenses vapor from the humid stream using a cooling water flow which minimizes the contaminants condensing by controlling the condensation temperature. The condensed water separates from the cooling water flow (6) and is usable as irrigation water as less than 1% contaminates by mass remain. The exhaust air contains a small amount of water vapor and most remaining contaminates.

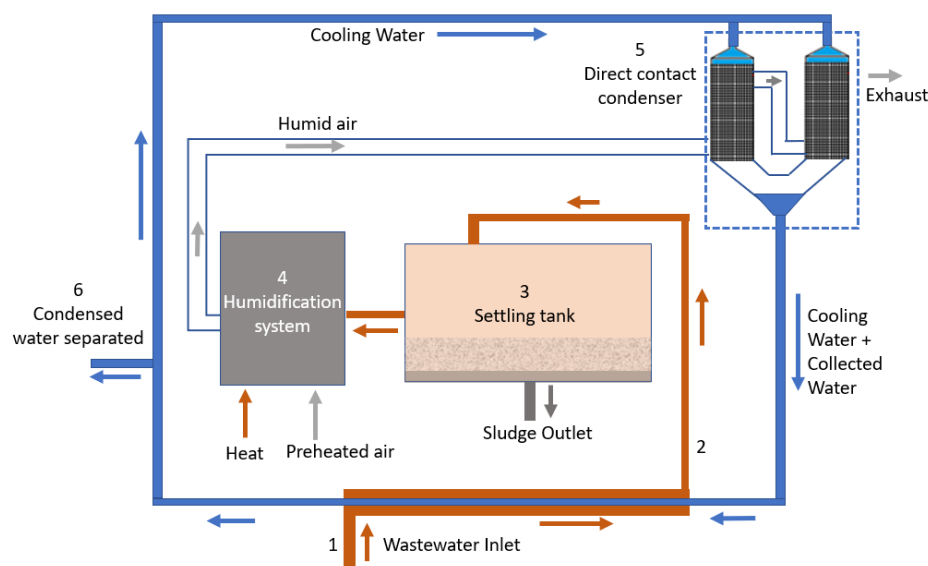


Figure 2.1 OSU's oil and gas wastewater purification system

2.1.2. Direct contact condenser

A direct contact condenser (DCC) works by putting a coolant in contact with a vapor. The coolant used in a DCC must be acceptable when coolant and vapor are mixed. Our system uses a packed bed condenser with two columns as shown in Figure 2.2. Note that this is a condenser packed bed, and it can be used as most of the solids are separated in the upstream, so minimal to no solid-state fouling occurs in the DCC's packed bed. In this packed bed condenser cooling water enters from the top and interacts with vapor within the bed where it is condensed and mixed with the cooling water. The exhaust air retains small amounts of vapor and most of the volatile contaminants. The performance of the DCC is based on the amount of vapor condensed. If the humid air temperature is too low the performance decreases while a high humid air temperature may increase performance. Humidity ratio is

the most important factor. A higher humidity ratio means there is a higher difference in temperature between the humid air dew-point and the cooling flow which leads to more effective condensation. It also means that the partial pressure of vapor is increased which increases the condensation temperature of the contaminants. The level of contaminants in the humid air should be minimized to prevent them from condensing with the freshwater. Avoiding the condensation of contaminants will not guarantee 100% pure freshwater, as a portion of contaminants will diffuse with water, but low cooling water temperature and low partial pressure of contaminants will decrease the amount that diffuses. The humidification system should be compatible with the DCC to improve the performance by providing humid air at high temperatures and high humidity ratios. Henry's law analysis was performed to determine the amount of gas that diffuses into a type and volume of liquid based on the partial pressure of the gas in equilibrium with that liquid. The analysis showed the water stream would have less than 2.5% contaminants after condensation.

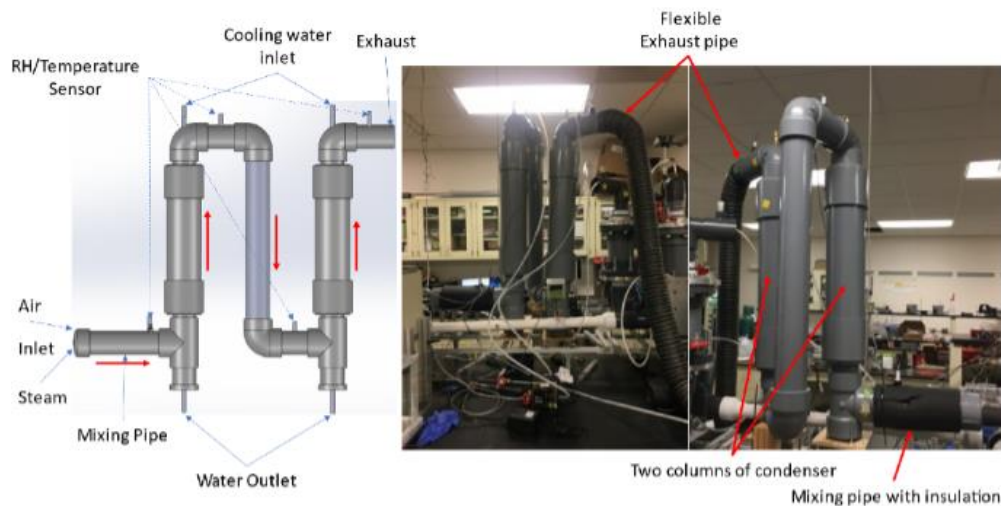


Figure 2.2 Schematic and CAD of the direct contact condenser

2.1.3. Humidification techniques

This paper will discuss two humidification techniques, spray humidification and venturi nozzle humidification both of which are used in HDH systems.

2.1.3.1. *Spray humidification*

Spray humidification is the method of humidifying air by mixing it with water spray. It can be operated at lower temperatures utilizing low-grade heat. Typically spray humidification is

achieved by using an air-assist or air-blast atomizer that allows water to flow through a center orifice and a jet of air to flow around the center orifice causing high shear breaking the water jet into small droplets. Generating spray from contaminated water such as oil and gas wastewater is difficult as any impurities in the water can easily foul the orifices deteriorating the humidification process. As an alternative to the traditional atomizer, our team has developed and patented an anti-clogging atomizer which has potential to atomize high salinity water (10% salinity) [5]. Our spray humidification design utilizes the anti-clogging atomizer which requires an air stream, preheated with low grade heat, flowing vertically through the anti-clogging atomizer to interact with the wastewater. If needed, a secondary air stream can be added in a counterflow configuration to increase the air moisture holding capacity to meet the desired humidity ratio target. The counterflow air also increases the interaction between all flows improving humidification. After the streams have mixed any unevaporated water can be discharged from the bottom and the humid air stream can continue to the DCC for dehumidification.

2.1.3.2. *Venturi nozzle humidification*

Humidification technologies commonly use a boiler to generate vapor from liquid that may or may not contain contaminants. The vapor is then mixed with heated dry air to humidify it. This process can be energy intensive as the latent heat of vaporization is much higher than sensible heat. In our HDH system the wastewater is transferred to an evaporation zone and once evaporated it enters a venturi driven mixing nozzle to mix with preheated air and form a humid air stream. One feature is the humid air outlet temperature is generally higher than that for spray humidification as the air and steam flows are above 100°C. This is advantageous as the carrying capacity of water increases with temperature, so less air is needed to transport water to the DCC.

2.2. **Energy consumption**

Energy is an important consideration for operation cost of a water treatment system. Lowering the cost to purify oil and gas wastewater will increase the quantity of water purified and conserve this resource. In 2010, the cost to transport oil and gas water to storage injection wells was \$2.1B [6]. If the cost to purify is less than the cost to transport, it will be more economical to purify than store and more water can be reused and recycled. Our system will produce water with 30% less cost compared to other existing approaches, such as

underground injection (storage), membrane, ion exchange etc. by producing purified water at $\$7/\text{m}^3$ [7].

2.2.1. Energy comparison

Experiments were conducted using the anti-clogging atomizer for spray humidification. As shown in Figure 2.3, ambient air flows through a flow meter and pressure transducer (A) before moving to the anticlogging atomizer (C). Pure feed water flows through a heater, flow meter, and pressure transducer (B) before flowing to the anticlogging atomizer. The counterflow air stream passes through a heater, flow meter, and pressure transducer (A) before reaching the top of the chamber. The humid air outlet was placed on the side of the chamber where the temperature and relative humidity are measured (E). Any unevaporated water is discharged (F) to keep the water in the chamber constant. Table 2.1 shows the data for tests where the feed water flow rate was 0.4 g/s, atomizer air flow rate was 0.4 g/s at 22°C, and the counter flow air flow rate was 0.4 g/s. For both tests the humid air leaving had 100% relative humidity and higher inlet conditions led to higher output temperatures.

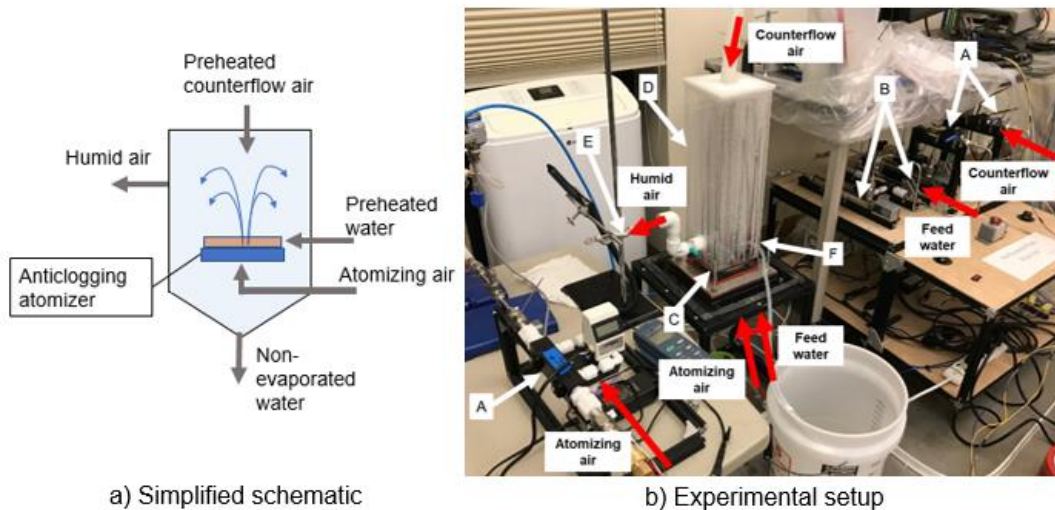


Figure 2.3 Experimental setup for spray humidification: a) simplified schematic b) experimental setup

Table 2.1 Experimental data for spray humidification

Test	Counter flow air temperature (°C)	Feed water temperature (°C)	Humid air temperature (°C)	Humid air relative humidity
1	60°C	29°C	25°C	100%
2	104°C	32°C	29°C	100%

The energy required for spray humidification was determined by calculating the change in enthalpy required to reach the experimental inlet conditions from ambient conditions. The only energy added during spray humidification was sensible energy to preheat the streams. The pumping power for both water and air streams were not included in this analysis as the difference is negligible between both humidification designs. For the data points shown in Table 2.1, the energy required for preheating the streams was 500 kWh/m³ and 816 kWh/m³ respectively.

Venturi nozzle humidification requires adding both sensible and latent heat. To directly compare the energy needed for the two systems, the vapor flow rate was maintained for both systems. The vapor flow rate was calculated using the humid air outlet temperature, relative humidity, and dry air flow rate from the incoming air streams. The energy required to produce the vapor flow rate of the two data points in Table 2.1 was 700 kWh/m³ and 990 kWh/m³. One energy reduction method is to operate venturi nozzle humidification with lower air flow rates decreasing the energy to preheat the air flow. The results of this experiment and energy analysis show that spray humidification can reduce the energy required to humidify the water by 20-30%. It should also be noted that in a boiling humidification system additional energy is required to preheat the air stream, which was not included above. For the same air flow rate but with an increased temperature of 120°C, to avoid condensation prior to the condenser, it requires an additional 1170 kWh/m³ which makes spray humidification 60-70% less energy intensive.

2.3. Contaminant separation

Oil and gas wastewater contains a variety of contaminants such as salts or dissolved chemicals which can require different separation methods. Suspended particles such as mud and clay can be removed via a settling tank. Some compounds like ethylene glycol and 2-

butoxy-ethanol can be removed through evaporation as they have a higher boiling point than water (less volatile).

2.3.1. Salt management

NaCl is the most common salt in oil and gas wastewater, but other salts may also be present, and the concentration varies from near freshwater to 14 times that of seawater [2], [8]. Salts are very corrosive and can cause fouling problems in an HDH system lowering the amount of water condensed and contaminants removed.

2.3.1.1. *Spray humidification - Salt management*

The antifouling atomizer, as proposed for use with the spray humidification system, has had no recorded fouling during use with high salinity water. Therefore, all fouling from salt in the humidification system can be avoided. However, ensuring that salt does not foul the DCC is a more complex issue. The wastewater, which contains salts, will be atomized producing a spray with both salt particles and water droplets. The salt particles could become entrained in the humid air stream and foul the DCC. According to Xuening et. al. [9] who modeled and tested brine spray evaporation using a traditional atomizer, if the air flow rate is too high the salt particles become separated from the brine and can be entrained within the humid air. But if air flow is too low, less energy will be available to evaporate water. The spray humidification design may need to be optimized to reduce salt entrainment by varying the atomizing air and counterflow air flow rates. One method to reduce the entrained salt from reaching the DCC is to add a cyclone after humidification. This could separate salt that is entrained by the humid air using the density gradient to remove salts before the DCC. However, it does increase the complexity of the overall design and the manufacturing cost.

2.3.1.2. *Venturi nozzle humidification - Salt management*

Evaporative humidification by nature does not allow any dissolved solids in the humid air stream. Venturi nozzle humidification provides a simple solution to removing salts that is common with current water treatment practices. As salts are unable to become entrained with the humid air there is a very low possibility that the DCC will become clogged/fouled, however, the heating element in the venturi nozzle humidification unit will be heavily prone to fouling and require other fouling mitigation techniques.

2.3.2. Azeotropes

An azeotrope mixture implies that the equilibrium composition of a mixture is unchanged through simple distillation. O'Hern et al. [2] reviewed various methods for the removal of azeotropes in wastewater. They suggest that temperature control in a HDH system of $\pm 1^\circ\text{C}$ of the thermal saturation temperature can remove up to 97.5% of water-based azeotropes [2]. The HDH system will control the temperatures of evaporation and condensation to selectively evaporate and condense the mixture to minimize the azeotropic contaminants. In a venturi nozzle humidification system, the evaporation temperature can be adjusted within 1°C of the saturation temperature reducing the quantity of azeotropes. However, in spray humidification the azeotropes will also be atomized which increases such compounds in the DCC. Further testing is required to determine how azeotropes react in spray humidification and what the increase in azeotropes in the final condensed water would be compared to venturi nozzle humidification.

2.4. System complexity

System complexity can greatly impact the overall performance and cost of a system. Additional components can increase the number of techniques required for contaminate separation, increase cost, and/or increase complexity of the control system. Both humidification designs require pumps and heaters for air and water streams. The spray system also requires a cyclone, as discussed in Section 2.3.1.1, which increases the overall complexity of the design. In addition, spray humidification increases the complexity of azeotrope removal in the DCC as discussed in Section 2.3.2. Venturi nozzle humidification may also require additional components such as a heat exchanger to recuperate energy and reduce operation cost which increases complexity.

Our HDH design will require a control method to monitor the flow rate of purified water and adjust both temperatures and flow rates to meet the required output. The controls will adjust parameters based on a model of the system and how that model reacts to changes in the operating conditions during operation. If venturi nozzle humidification is chosen, the control system will also adjust the heat input for evaporation. Modeling the spray humidification design may be more complex as the liquid-gas interaction is more complex than that in venturi nozzle humidification. Modeling for spray humidification has primarily been done for water that did not contain salts or other contaminants. For example, Xuening et. al. [9] produced a CFD model for a brine spray that was within 5% of experimental values but this

model did not include other contaminants. However, if a model is produced for spray humidification that can accurately predict the system's response with all contaminants the control of the system will not be very different from venturi nozzle humidification.

2.5. Conclusions

In conclusion, both spray and venturi nozzle humidification systems have potential in our HDH purification system, and both can produce clean water for reuse. Spray humidification can reduce energy costs by up to 70% and reduce fouling in the humidification system with the antifouling atomizer developed at Oregon State University. It can also avoid salt contamination in the direct contact condenser (DCC) if paired with a cyclone, but it increases the design complexity. By contrast, venturi nozzle humidification can control the temperature of evaporation which will prevent the salt in oil and gas wastewater from being evaporated and entrained in the humid air. Venturi nozzle humidification requires more energy and reducing the energy introduces more complexity and controls requirements. Future research will expand the range of salinities, contaminants, and temperature ranges tested for both systems and develop an experimentally validated model to calculate the energy required for each system.

Author Contributions

Morgan Messer and Xiang Zhang prepared the experimental setup and conducted experiments collecting data. Morgan Messer processed experimental data. Morgan Messer, Xu Tan, and Bahman Abbasi formulated the paper. All authors conceived and designed the study, approved the final version of the manuscript, and agree to be held accountable for content therein.

References

- [1] S. J. Maguire-Boyle and A. R. Barron, "Organic compounds in produced waters from shale gas wells," *Environmental Science: Processes & Impacts*, no. 10, 2014.
- [2] H. O'Hern, E. Nikooei, X. Zhang, C. Hagen, N. AuYeung, D. Tew and B. Abbasi, "Reducing the Water Intensity of Hydraulic Fracturing: A Review of Treatment Technologies," *Desalination and Water Treatment*, vol. 221, pp. 121-138, 2021
- [3] S. M. Zubair, M. A. Antar, S. Elmutasim and D. U. Lawal, "Performance evaluation of humidification-dehumidification (HDH) desalination systems with and without heat recovery options: An experimental and theoretical investigation," *Desalination*, vol. 436, pp. 161-175, October 2017.
- [4] B. Abbasi, X. Zhang, H. O'Hern and E. Nikooei, "METHOD AND SYSTEM FOR PURIFYING CONTAMINATED WATER". United States Patent 62882970, 4 August 2020.

- [5] B. Abbasi, M. A. Khalifa Elhashimi, D. Sharma and X. Zhang, "METHOD AND APPARATUS FOR DESALINATING WATER". United States Patent 245-102688-01, August 2019.
- [6] T. Silvia, S. Morales-Torres, S. Castro-Silva, J. Figueiredo and A. Silvia, "An overview on exploration and environmental impact of unconventional gas sources and treatment options for produced water," *J Environ Manage*, vol. 200, pp. 511-529, 2017.
- [7] M. Schantz, "Produced and flowback water treatment from fracking," *Unconventional Oil and Gas Symposium*, 2014.
- [8] A. Fakhru'l-Razi, A. Pendashteh, D. Radiah Awang Biak, L. Chuah Abdullah, S. Siavash Madaeni and Z. Zainal Abidin, "Review of technologies for oil and gas produced water treatment," *Journal of Hazardous Materials*, vol. 170, no. 2-3, pp. 530-551, 2009.
- [9] F. Xuening, C. Lei, D. Yuman, J. Min and F. Jinping, "CFD modeling and analysis of brine spray evaporation system integrated with solar collector," *Desalination*, vol. 366, pp. 139-145, 2015.

CHAPTER 3: Surface roughness fouling with mixed salts

Morgan Messer¹, Kyle Anderson¹, Xiang Zhang², Bahman Abbasi^{1*}

¹Oregon State University, 1500 SW Jefferson Way, Corvallis, OR 97331, USA

²Oregon State University-Cascades, 1500 SW Chandler Ave, Bend, OR 97702, USA

* Corresponding author: AbbasiB@oregonstate.edu

Journal of Heat Transfer, 2022

Submitted – under peer review

Effect of surface roughness on mixed salt crystallization fouling in pool boiling

Abstract

Desalinating saline water is one approach to producing freshwater to help meet increasing water demand. Desalination technologies face challenges (particularly on heat exchanger surfaces) with fouling causing lower heat transfer efficiency and lower freshwater yield with fixed energy input. Few studies have focused on multiple salt high-salinity solutions (well above seawater) in a pool boiling environment. This study investigates how heat exchanger surface roughness effects fouling resistance, heat transfer coefficient, and salt composition in a pool boiling environment with highly saline water (20% by mass), with/without an added organic compound (3% ethylene glycol). The heat exchange surface roughness was varied between an average surface roughness of 0.35 μm , 5 μm , and a microchannel surface (common in boiling systems) with average surface roughness of 10.5 μm . The 0.35 μm surface had a 1.5 $\text{cm}^2\text{K/W}$ lower fouling resistance compared to the other tested surfaces. 5 μm and 10.5 μm heat exchange surfaces had nearly identical heat transfer performance with fouling resistances of 2.7 $\text{cm}^2\text{K/W}$. Decreasing the surface roughness reduces fouling for smooth surfaces (0.35 μm), but if is sufficiently rough (5 - 10.5 μm) it has minimal impact on fouling. 3% ethylene glycol (found in antifouling coatings) was added to the solution but had no apparent effect on the fouling resistance or heat transfer coefficient, however it did affect what salts were formed. The information from this study will help optimize future heat exchange surfaces for treating high-salinity water in desalination.

Keywords: Saline, Desalination, Fouling, Crystallization fouling, Surface roughness, Ethylene glycol

3.1. Introduction

The demand for water is increasing due to industrialization, higher standards of living, and population growth. Increasing demand combined with the depletion of natural freshwater resources has led to water scarcity in many countries around the world. According to the United Nations Water Organization [1], over 2.3 billion people experience high water stress

at least one month per year. Desalination technologies present an opportunity to meet the increasing demand and eliminate water scarcity. Many desalination systems use a membrane or thermal based distillation approach. Thermal based approaches commonly evaporate seawater using a heating element and then condense that water, leaving salts and other impurities behind.

Fouling, or material surface deposits, are problematic in desalination technologies. Fouling deposits can lower heat transfer efficiencies, increase piping pressure drops, and increase corrosion leading to increased maintenance costs in desalination systems [2], [3]. The five main fouling types are: biological, corrosion, particulate, chemical, and crystallization fouling. Crystallization, or scale, fouling accounts for 70% of total fouling in desalination systems, as seawater is primarily inorganic [2]. As salts have low thermal conductivity (0.5-2 W/mK), fouling buildup reduces the heat transfer coefficient between the heater and saltwater leading to a reduction in the system's overall efficiency. Crystallization fouling is dependent on momentum, velocity, heat and mass transfer, chemical kinetics, surface material properties, heating configuration, surface temperature, and concentration which makes it difficult to predict [3], [4], [5], [6]. Studies have been done to understand the influence of various parameters on fouling accumulation.

3.1.1. Salt concentration and types

Crystallization fouling is highly dependent on the degree of salt supersaturation in a solution due to an increase in potentially fouling salts, fouling rates, and nucleation sites available for crystals to attach to and grow [3], [7]. Increasing calcium chloride concentration increases the fouling resistance and shortens the induction time (duration when fouling resistance is greater than nucleation site enhancement) [8]. Many studies have investigated fouling with low salinity solutions (0.0034 - 0.4%), but few have studied fouling characteristics in saline solutions higher than 0.4% [3], [4], [5], [9]. Many desalination plants produce highly saline (brine) as a byproduct of the desalination process, but brine treatment technologies are not cost effective compared to cheaper, and more environmentally damaging disposal methods [10]. To improve high salinity desalination efficiency and extract the maximum amount of water fouling behavior in highly saline environments needs to be understood.

Different salts have different adherence, solubility, and heat transfer characteristics. The solubility characteristics of different salts impacts the fouling quantity and fouling rate. Salts with decreased solubility at higher temperatures generally begin crystallization fouling [11].

Calcium sulphate and calcium carbonate fouling has been extensively studied as they commonly foul heated surfaces causing fouling resistances of $7 \text{ cm}^2\text{K/W}$ after 100 hours in subcooled boiling conditions [3], [4], [8], [12]. While these salts have been well studied, there has been limited research on multiple salt mixtures and how their interactions influence fouling.

Helalizadeh et. al. [3] studied a mixture of calcium sulphate (CaSO_4) and calcium carbonate (CaCO_3) fouling in a subcooled flow boiling system. They showed that mixed salts have more fouling accumulation than individual salts in 66% of the concentrations tested and the highest accumulation occurred with a mixture of salts [3]. Song et al. [13] compared the fouling resistance of CaCO_3 and CaSO_4 in different concentrations and found in 75% of the tested cases mixed salt fouling was higher than individual salt fouling. This indicates more studies are needed on multiple salt solutions as desalination systems rarely treat water with 1-2 salts and additional salts change the overall fouling behavior.

3.1.2. Surface roughness effect on fouling

Increased surface roughness impacts both boiling characteristics and fouling accumulation. MacAdam and Parsons [14] found that increasing the average surface roughness (R_a) by $0.6 \mu\text{m}$ caused an increase in fouling even in a limited ($0.2\text{-}0.8 \mu\text{m}$) surface roughness change. It also increases deposit adhesion- up to 30X more stress is required to remove CaCO_3 and CaSO_4 fouling from a rough versus a smooth surface ($0.1\text{-}21 \mu\text{m}$) [6], [15]. However, for a smaller change in surface roughness ($0.018\text{-}0.246 \mu\text{m}$), Lui et. al. [16] found that smoother surfaces did not show fouling or adhesion reduction for $\text{Ca}(\text{HCO}_3)_2$ fouling. Fouling adhesion is important as many crystallization fouling resistance curves reach a plateau where the fouling accumulation rate and the removal rate due to flow shear stress is equal. Surface roughness manufacturing techniques and geometries should be considered as they may have the same roughness value but different impacts [17].

The impact of various roughness values on nucleate boiling have been studied for average surface roughness (R_a) of $0.04\text{-}1.5 \mu\text{m}$ systems [18]. Rougher surfaces have increased phase change heat transfer due to increased agitation from improved bubble formation [18]. Jones et. Al. [19] studied the effect various surface roughness had on pool boiling heat transfer in pure water and found no additional benefit to increased average surface roughness for $1.08 \mu\text{m}$ to $10 \mu\text{m}$; but did not consider how this would affect fouling [19]. As fouling occurs, the depositions can change the surface roughness of a material, thus impacting other factors that affect fouling accumulation. For example, as salts begin to accumulate in a tube, they

increase the surface roughness and restrict the flow volume, thus accelerating the flow which can help compensate for the heat transfer reduction from the increased fouling resistance and the increased friction factor [17]. In addition, surface coatings have been one area of interest to reduce fouling as they can change the surface characteristics (roughness, hydrophobicity, etc.) but they can come at a cost due to the added resistance of the material itself, may degrade over time, and may only work for specific materials [20], [21].

3.1.3. Boiling effect on fouling

During boiling with crystallization fouling, salt deposits can temporarily increase the heat transfer rate due to increased nucleation sites and near wall turbulence; however, overtime the increase in nucleation sites cannot overcome the fouling resistance and the heat transfer rate decreases [11], [17]. Many studies have focused on fouling in subcooled boiling environments, despite evidence showing fouling accumulation is a much larger issue in pool boiling situations due to the bubble formation mechanisms and detachment [3], [9], [12], [22]. Subcooled boiling is common in heat exchangers as boiling only occurs on the heated surface, but the bulk of the fluid is subcooled. Forced convection in subcooled boiling has a significant impact on the rate of fouling accumulation compared to pool boiling [9]. While subcooled boiling and fouling in convective heat transfer have been studied, there is limited information available for mixed salt, high salinity fouling during pool boiling.

Fouling in a pool boiling system occurs due to bubble formation and micro-layer evaporation. Therefore, methods used to increase bubble formation to improve boiling efficiency will also increase crystallization fouling on the heated surface [9]. As bubbles form on the heated surface, the bubble's interface becomes supersaturated which results in salt deposits on the surface. Raghupathi & Kandlikar [5] studied fouling formation on a flat heat transfer surface in a pool boiling experiment using artificial seawater (0.0034% wt. salt). They found that boiling seawater compared to pure water increases the CHF due to increases in nucleation site density from fouling accumulation. Crystallization fouling also added thermal resistance causing the wall superheat to increase [5]. Jamialahmadi and Müller-Steinhagen compared pure water and 0.1% salinity calcium sulfate solution in pool boiling characteristics and found that the bubble departure diameter was increased for saline solutions and the heat transfer coefficient changes based on bubble formation mechanisms [22]. The presence of salt causes a porous layer which can cause the boiling to resemble wick boiling with multiple steam channels through the salt layer [22]. Understanding how the surface and pool boiling

mechanisms are changed with the presence of a porous adhered salt layer is important to understand how boiling seawater with different heating surfaces and higher salinities impacts the fouling accumulation for mixed salts.

3.1.4. Ethylene glycol effect on fouling

Understanding the importance of salt mixtures and surface roughness is necessary to better design evaporators and heat transfer surfaces in desalination units. It is equally important to understand how the presence of other compounds present in a saline solution affect the fouling resistance and heat transfer coefficient. Several studies have found that a polyethylene glycol (PEG) based coating on a membrane can be used to reduce crystallization and biological fouling in seawater systems [23], [24], [25]. PEG is created after ethylene glycol reacts with itself in water creating a variety of ethylene glycol units which are soluble in many organic solvents. PEG is found in many commonly used products [23], [26]. While there has been success with creating ethylene glycol-based surface coatings to mitigate fouling in reverse osmosis' processes, these coatings have had minimal use in evaporation-based desalination systems. Furthermore, there is limited information on whether ethylene glycol dissolved in a water-based solution has the same effect as a surface coating and if it could be utilized for its antifouling properties outside of a reverse osmosis-based desalination system.

A new technology from Oregon State University uses a humidification dehumidification process to treat hydraulic fracturing wastewater (20% salinity with other compounds including 3% ethylene glycol) [27], [28], [29]. If ethylene glycol can be separated during desalination, and if it reduces fouling, this could indicate if desalination techniques can be used to treat highly contaminated wastewater. Nikooei et. al. [29] using a representative hydraulic fracturing mixture found evaporation separated most contaminants including ethylene glycol. There was no mention of how additional solution contaminants affected crystallization fouling which requires further research. This report addresses the affect ethylene glycol has on crystallization fouling in a highly saline solution (20%).

3.1.5. Current work

Fouling accumulation changes based on salt, time, flow rate, surface properties, heat and mass transfer, temperature, concentration etc. making it difficult to predict. These characteristics have been studied for specific situations with low salinities, subcooled boiling systems, and single salt solutions [3], [4], [5], [9]. Limited information is available for high

salinity fouling with more than two mixed salts in pool boiling conditions on various surface roughness'. Understanding how the mentioned conditions effect fouling accumulation can be utilized to effectively treat high salinity solutions that are a byproduct of desalination and is often untreated. The brine naturally contains multiple salts, and salt mixtures have different fouling characteristics compared to single salt solutions [3]. Estimating the fouling resistance on different heating surfaces during operation is important to track changes to the efficiency and operation and maintenance costs associated with high salinity mixed salt fouling. The present study focuses on determining the heat transfer fouling resistance on a vertical heating surface in a high-salinity mixed salt pool boiling environment. It is designed to isolate the effect of surface roughness on fouling resistance by testing several heating surface roughness values (homogeneous surface roughness' of 0.35 μm and 5 μm , and a heterogeneous surface with microchannels with an average surface roughness of 10.5 μm). The microchannel 10.5 μm surface roughness test was repeated with an additional 3% ethylene glycol in the solution to determine the effect on fouling as ethylene glycol is used in antifouling coatings and found in many products, as minimal studies have considered the effect when the ethylene glycol is in the solution.

3.2. Experimental setup

Figure 3.1 shows the experimental and actual setup used in the current study. A cartridge heater (120 V, 500 W) is embedded into a 115 mm x 50 mm x 50 mm aluminum 6061 block which is submerged in saline water. Aluminum was chosen as aluminum has higher fouling accumulation compared to brass and stainless steel and therefore presents fouling much quicker and reduces the standard multiple day experiments to a few hours [4], [14]. Using aluminum also prevents corrosion issues that would have occurred with ferrous heat exchangers. The cartridge heater was controlled with a Belee 20 A variable voltage transformer and power was measured with a Baldr power meter. The heater power was fixed at 200 W and recorded every 30 minutes. The aluminum block has 16 Type K thermocouples embedded 25 mm into the block to measure the block's temperature radially and avoid any temperature bias from hot spots (Figure 3.1B). The embedded thermocouples holes were filled with Boron Nitride thermal paste and sealed with Dowsil RTV sealant to avoid water interacting with the embedded thermocouples. Silicone rubber was also used to secure insulation (Superwool plus MD paper) to the bottom of the block to avoid heat losses to the water through the bottom surface and a thermocouple was embedded on outside of the insulation to ensure it was preventing heat loss as intended. During the 2.5-hour tests, the

measured temperatures were below the block temperature justifying that the bottom area could be neglected in the fouling resistance analysis as focus was on the radial temperature distribution.

The aluminum block's roughness was adjusted between tests to achieve average Ra values of 0.35 μm , 5 μm , and 10.5 μm measured with a profilometer (Mitutoyo SJ-201). Sandpaper was used to achieve the homogeneous 0.35 μm and 5 μm surface roughness' (Figure 3.2). A Dremel was used to cut shallow horizontal and vertical lines in a grid pattern to achieve microchannels with an average surface roughness of 10.5 μm as these are common in boiling systems (Figure 3.2).

The saline mixture was continuously mixed using a magnetic stirrer before being pumped into the testing chamber using a Masterflex L/S displacement pump to control the flow rate. At the top of the chamber there are openings for vapor to escape. The flow rate was adjusted to compensate for the evaporated water and keep the block's surfaces submerged. Two RTDs were located on opposite sides of the block 5 mm from the block's surface and 50 mm from the top to be inline with the embedded thermocouples to measure the water temperature. All thermocouples and RTD temperatures were recorded using an Agilent 34970A DAQ. The power meter, thermocouples, and RTD measurements are used to determine the thermal resistance and heat transfer coefficient due to fouling. After the experiment the saline water was removed from the excess discharge port. The surface was thoroughly cleaned between tests to remove all salts and ethylene glycol.

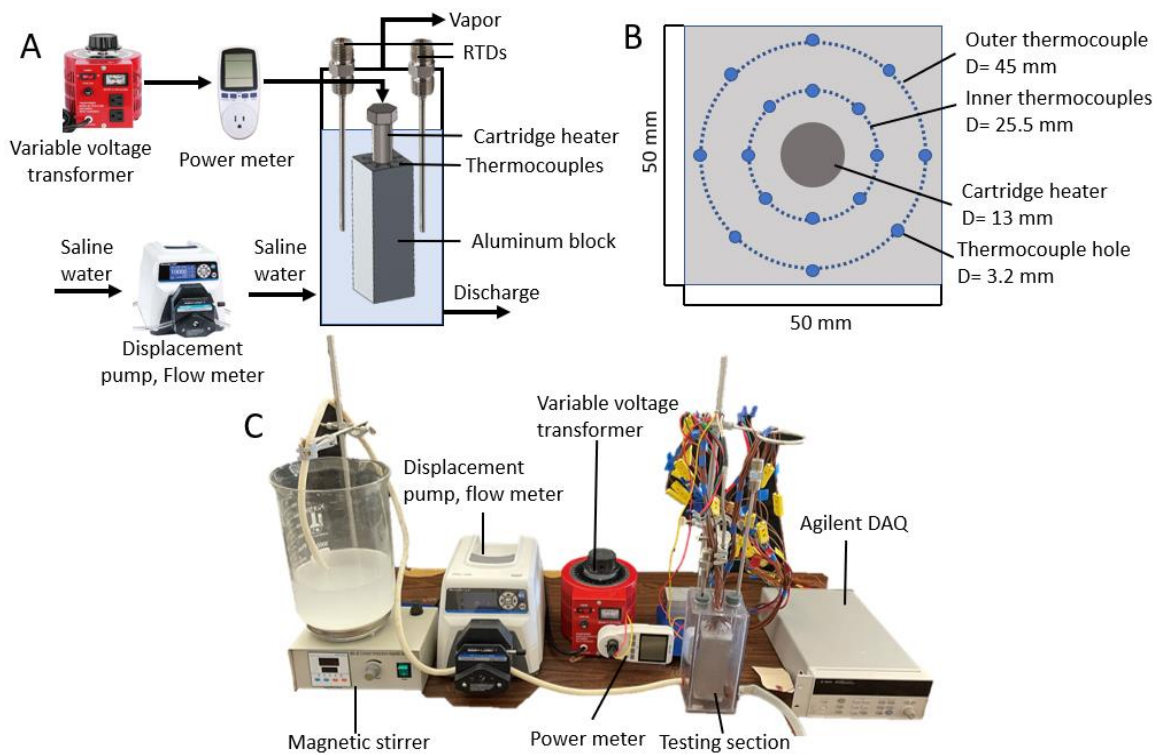


Figure 3.1. Experimental setup used to determine the fouling resistance and the heat transfer coefficient for various surface roughness and solutions A) experimental schematic, B) schematic showing the top view of the aluminum block, C) actual setup

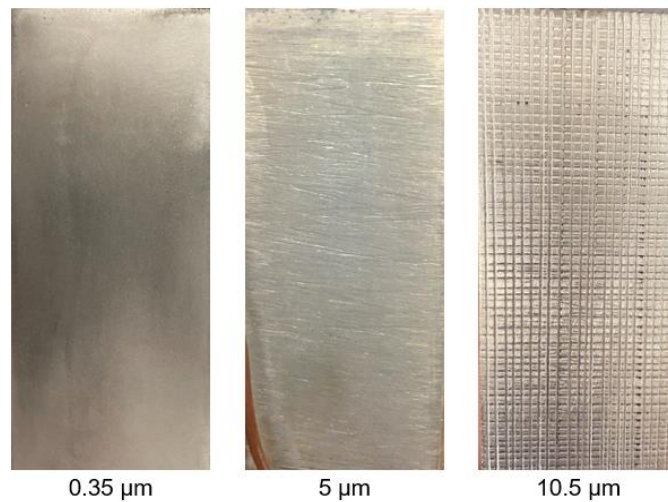


Figure 3.2. Aluminum block with different roughness, 0.35 μm and 5 μm were achieved using sandpaper creating a homogeneous surface roughness, and 10.5 μm was achieved with a Dremel creating microchannels and a heterogeneous surface

The saline water was mixed to match seawater (Sea Salt ASTM D1141-98, n.d. [30]) as shown in Table 3.1 (salts with less than 1% concentration in seawater were neglected). The total salts were scaled to create 20% saline water for tests as shown in Table 3.2. Using 20% saline water reduces the total test time as fouling occurs quickly and ensures each test is focused on heating/evaporating processes that manage brine or highly saline solutions. A test matrix with operation parameters for all experiments conducted is shown in Table 3.3. Each experiment in Table 3.3 was conducted 3 times to ensure repeatability.

Table 3.1. Salts used in a representative seawater composition (Sea Salt ASTM D1141-98, n.d. [30])

Compound	Symbol	Weight Percentage
Sodium chloride	NaCl	58.5%
Magnesium chloride	MgCl ₂ - 6H ₂ O	26.5%
Sodium sulfate	Na ₂ SO ₄	9.8%
Calcium chloride	CaCl ₂	2.8%
Potassium chloride	KCl	1.6%
Other salts	---	0.8%

Table 3.2. Testing solution for experiments with and without Ethylene glycol

Compound	Brine 1 (No Ethylene-glycol) (wt%)	Brine 2 (with Ethylene-glycol) (wt%)
Water	80.1%	77.8%
Sodium chloride	11.7%	11.4%
Magnesium chloride	5.3%	5.2%
Sodium sulfate	2%	1.9%
Calcium chloride	0.6%	0.5%
Potassium chloride	0.3%	0.3%
Ethylene-glycol	0	2.9%

Table 3.3. Surface roughness crystallization fouling experimental test matrix

Experiment number	Salinity (wt %)	Ethylene glycol (wt %)	Average aluminum surface roughness (μm)
1	20	0	0.35, homogeneous
2	20	0	5, homogeneous
3	20	0	10.5, microchannel
4	20	3	10.5, microchannel

To determine which salts attributed to the crystallization fouling, the attached salts were removed from the aluminum block by dissolving the adhered salts in distilled water. Once all salts had been removed and dissolved in the water, the water was evaporated leaving behind only the salts that had attributed to the crystallization fouling. The accumulated salts from the tests with and without 3% ethylene glycol in the solution were analyzed using ICP-OES (inductively coupled plasma optical emission spectrometry). Nitric acid was used as the diluent in this process to determine which elements were present in the crystallization fouling.

3.3. Methodology

The methodology used to analyze the data is consistent with literature. To determine the fouling resistance, R_f , between the heat exchange surface and the saline water solution, Eq. 1 was used.

$$R_f = \frac{1}{h_f} - \frac{1}{h_0} \quad (1)$$

where h_f is the heat transfer coefficient between the heat exchange surface and boiling water as fouling occurs, and h_0 is the initial heat transfer coefficient at the beginning of the test. h_f and h_0 are calculated using Eq. 2 and Eq. 3 where q'' is the heat flux produced by the heater. q'' was assumed to be uniform throughout the block. $T_{s,f}$ and $T_{w,f}$ are the surface temperatures of the heat exchange surface and the water, respectively, as fouling occurs. $T_{s,0}$ and $T_{w,0}$ are the temperatures of the heat exchange surface and the water at the beginning of the test before

any fouling has occurred. To provide a clear comparison between tests, all h_o values reference when $T_{w,0} = 101^\circ\text{C}$.

$$h_f = \frac{q''}{T_{s,f} - T_{w,f}} \quad (2)$$

$$h_o = \frac{q''}{T_{s,0} - T_{w,0}} \quad (3)$$

The heat flux, q'' , is calculated by dividing the measured heater power, read from the digital power meter, by the surface area of the aluminum block that was in contact with the saline water. The heat transfer surface area only included the sides of the block as the top and bottom of the block were insulated forcing all the heat to exit through the sides of the block. Both water temperatures, $T_{w,0}$ and $T_{w,f}$, were measured as the average of the two RTDs that were submerged roughly 50 mm under the surface of the boiling water. The surface temperatures of the block, $T_{s,0}$ and $T_{s,f}$, were calculated using the average of the corner and middle thermocouple measurements for each side. The average side temperature was averaged over all four surfaces to calculate the average surface temperature for the whole block. Each side of the block's surface temperature was calculated using a Eq. 4 based on the outer most thermocouple temperature and the measured heat flux.

$$T_s = T_{TC,o} - q'' \cdot R_{al,o} \quad (4)$$

q'' is the heat flux provided by the heater, $T_{TC,o}$ is the outer ring thermocouple reading, and $R_{al,o}$ is the thermal resistance between the outer thermocouple and the surface of the block. $R_{al,o}$ is calculated using Eq. 5

$$R_{al,o} = \frac{D_{al,o}}{k_{al}} + \frac{D_{tp}}{k_{tp}} \quad (5)$$

where $D_{al,o}$ is the thickness of aluminum in between the edge of the outer thermocouple hole and the edge of the block, D_{tp} is the radius of the hole that the thermocouple was inserted into (filled with thermal paste), and k_{al} and k_{tp} are the thermal conductivities of aluminum and the thermal paste used to fill the thermocouple holes respectively.

To ensure that the power meter measurements were accurate, the heat flux, q'' , was also calculated by an alternative method. Using the temperature difference between each set of the inner and outer thermocouples ($T_{TC,i}$ and $T_{TC,o}$ respectively), and the thermal resistance between each set of thermocouples, $R_{al,i}$, q'' was calculated as shown in Eq 6.

$$q'' = \frac{T_{TC,i} - T_{TC,o}}{R_{al,i}} \quad (6)$$

Next, each of the q'' values calculated from the thermocouple temperatures were compared to the q'' values measured from the power meter. These two methods of measuring the heat flux produced results that matched within the uncertainty associated with the temperature measurements. As the heat flux values measured from each method produced matching results, the power meter's readings were used to determine the fouling resistance.

3.3.1. Simulation results

To validate the uniform heat flux assumption, the measured thermocouple values were compared to simulated values calculated by a SOLIDWORKS simulation that assumed a uniform heat flux from the heater's surface. The thermal FEA simulation used the water temperature (measured by the RTDs) and the power (measured by the power meter) to calculate the radial heat distribution. Figure 3.3 shows the temperature distribution across a cross-section of the aluminum block for a uniform heat flux boundary condition applied to the cartridge heater-block interface, and a constant temperature boundary condition applied to the outer heat transfer surface that was in contact with the boiling saline solution. These boundary conditions applied to the cross section of the aluminum block yielded a small temperature distribution (4°C) across the block. The white dots on Figure 3.3 represent the location where the SOLIDWORKS temperature solutions were compared to the actual thermocouple measurement from the experimental data. The simulation matched the measured thermocouple readings within 2-4%, thus validating the uniform heat flux assumption used to calculate the fouling resistance and heat transfer coefficient.

A mesh independence study was conducted for mesh sizes between 0.5-2 mm and found a change in error between the simulated and experiential temperatures to be very low (0.03-0.66%). To reduce computational power and maintain adequate accuracy, a mesh size of 0.75mm was used to simulate the temperatures with a uniform heat flux.

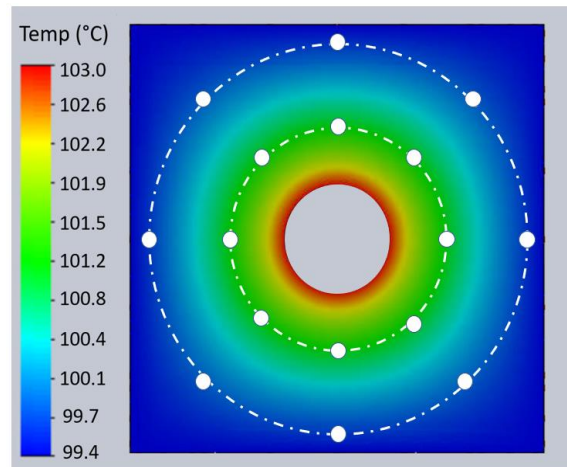


Figure 3.3. SOLIDWORKS simulation showing radial temperature distribution for $q''=66,000 \text{ W/m}^2$ and 97.4°C water temperature. 2-4% error compared to measured thermocouple data

3.3.2. Uncertainty propagation

The RTDs were calibrated by recording the reference resistance, R_0 , during an ice bath, and then averaging this reference resistance over 3 separate ice bath tests. Using the average reference resistance value from the ice bath tests, the temperature was calculated using Eq. 7 by applying the A and B coefficients provided by the RTD manufacturer. After calibration, the RTD uncertainty was determined to be $\pm 0.125^\circ\text{C}$. Type K thermocouples were calibrated by comparing the calibrated RTD temperatures to the thermocouple readings in both an ice bath and a hot water bath. This was done to account for any offsets in the thermocouple readings. After calibration, all the type K thermocouples showed an uncertainty of $\pm 0.5^\circ\text{C}$. If any of the 16 thermocouples failed (readings were not read properly by the DAQ) during the test, an average of the two adjacent thermocouples was taken as there were minimal differences in temperature measurements along the same radius.

$$R(T) = R_0 (1 + A \cdot T + B \cdot T^2) \quad (7)$$

The uncertainty from each of the measured values was propagated using the Kline-McClintock method implemented in Engineering Equation Solver (EES). The uncertainties included both measurement and precision uncertainty. As boiling is random in nature, many of the temperature measurements during the middle of the test had high variation between the 3 repeated tests. As the overall temperature changes, and by extension, fouling resistance over the course of the entire test was the most substantial finding from this work, only the

average temperatures of the first and last 5 minutes of each test were used to calculate the precision uncertainty associated with the repeated tests. Quantization uncertainty associated with the DAQ sampling rate was calculated for each sensor, but they were found to be insignificant compared to the other uncertainties. The final uncertainty values for all measured and calculated values are shown in Table 3.4.

Table 3.4. Uncertainty values for all measured values used in data analysis

Parameters	Uncertainty		
	Minimum	Average	Maximum
Thermocouple (°C)	-	0.5	-
RTD (°C)	-	0.1	-
Heater power (W)	-	3.5	-
Fouling Resistance (cm ² K/W)/%	0.440/11.7	0.503/23.9	0.607/60.7
Heat transfer coefficient (W/cm ² K)/%	0.008/3.2	0.019/9.8	0.046/17.7

3.4. Results and discussion

3.4.1. Temperature difference

Figure 3.4 shows the difference between the wall temperature and the water temperature during the experiment. As the water temperature is consistent during the test the change in the temperature difference is due to an increase in wall temperature from fouling accumulation decreasing heat transfer. The temperature difference between the 5 μm and 10.5 μm microchannel is very minimal meaning the wall temperature increase was the same and thus likely the same fouling accumulation occurred between tests. Whereas the 0.35 μm test had a much lower change in temperature indicating that minimal fouling accumulation occurred. This is important as this difference is used to calculate the heat transfer coefficient and fouling resistance, so the temperature difference is a good indicator to the amount of fouling accumulation and resistance present on the heater surface.

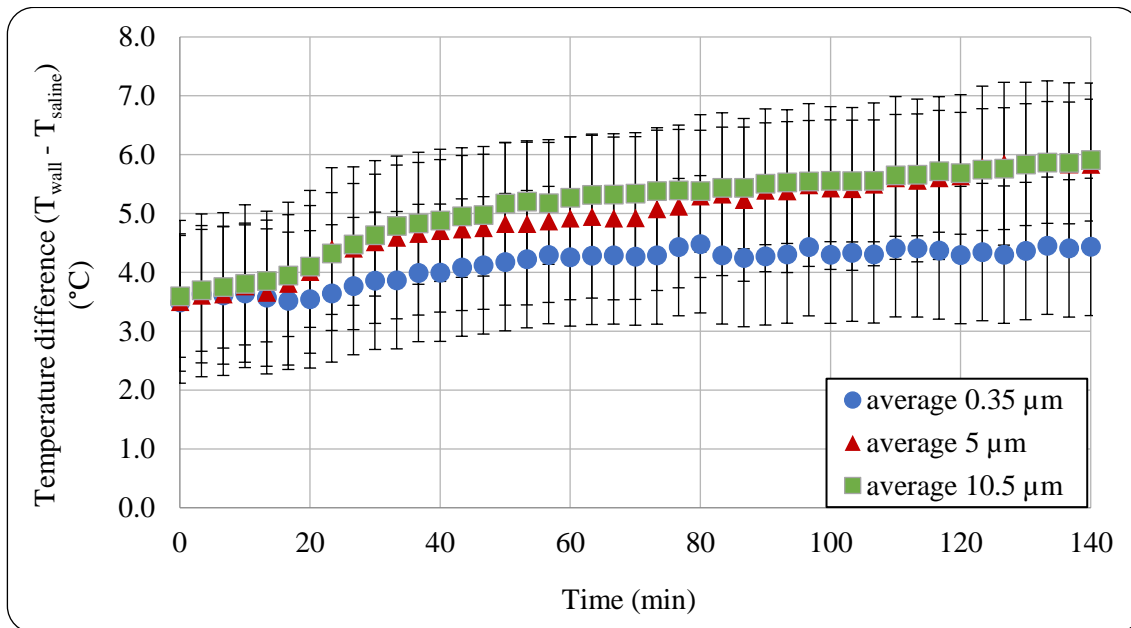


Figure 3.4. Impact of surface roughness on fouling resistance

3.4.2. Effect of surface roughness on fouling

Figure 3.5A shows the effect of surface roughness on both the fouling resistance and the heat transfer coefficient. The trend for all tests is consistent with literature as there is some initialization period that occurs in approximately the first 20 minutes of testing [3], [9], [11]. As show in Figure 3.5B the 0.35 μm test's heat transfer coefficient increases and the fouling resistance decreases which is due to the increased nucleation sites, increased surface roughness with small traces of fouling, and increased boiling. After this initialization period (first 20 minutes of testing) the fouling resistance dominates over the increased nucleation site as more salts accumulate on the surface. This graph also shows a linearly increasing trend for both the 5 μm and 10.5 μm (microchannel) tests throughout 140 minutes indicating the fouling has strong adhesion and the fouling removal rate (due to boiling stress) is lower than the fouling accumulation rate. Whereas the 0.35 μm test has an increasing trend for the first 60 minutes before plateauing indicating that fouling is asymptotic meaning that the increase in deposits and the removal of deposits from the shear stress of boiling occurring is equal and the deposits are weaker compared to other cases. This also indicates that a constant fouling resistance of 2 cm²K/W would be a good estimate for a system with a heating surface of 0.35

μm roughness, whereas a constant value for the $5\ \mu\text{m}$ or the $10.5\ \mu\text{m}$ test would be inaccurate for modeling operations as the fouling resistance is increasing with time and is not constant.

In Figure 3.5A, the fouling resistance for the $0.35\ \mu\text{m}$ surface increases about $1\ \text{cm}^2\text{K/W}$ in 120 minutes while the $5\ \mu\text{m}$ and $10.5\ \mu\text{m}$ surface roughness increases the resistance by $2.7\ \text{cm}^2\text{K/W}$. The $5\ \mu\text{m}$ homogeneous surface roughness and $10.5\ \mu\text{m}$ microchannel surface roughness had nearly identical values and trends for the heat transfer coefficient and fouling resistance indicating that the additional surface roughness from the addition of microchannels in the $10.5\ \mu\text{m}$ microchannel test had no impact on the fouling accumulation. There is also no benefit from reducing a heater's surface from $10.5\ \mu\text{m}$ with microchannels to a homogeneous surface roughness of $5\ \mu\text{m}$. But there is benefit of reducing the surface roughness from $5\ \mu\text{m}$ to $0.35\ \mu\text{m}$. With surface roughness' larger than $10.5\ \mu\text{m}$, we would expect to see fouling accumulation increase with surface roughness as the number and size of the nucleation sites changes and surface roughness becomes a more dominant indicator of fouling. Reducing the average surface roughness can decrease the effect that the surface roughness has on fouling accumulation if it is sufficiently reduced ($5\ \mu\text{m}$ to $0.35\ \mu\text{m}$) but reducing the surface roughness does not mitigate fouling when the surface is sufficiently rough.

Figure 3.5B shows the effect of surface roughness on the heat transfer coefficient. All three tests have very similar trends and values for the heat transfer coefficient indicating that the surface roughness has only a small impact on this value. The heat transfer coefficient mirrors the fouling resistance values in that they plateau after 60 minutes indicating the heat transfer coefficient is constant after sufficient fouling has occurred. The $5\ \mu\text{m}$ and $10.5\ \mu\text{m}$ tests had slightly lower ($0.05\ \text{W/cm}^2\text{K}$) heat transfer coefficients even initially when minimal fouling was occurring. This is counter intuitive as generally the rougher the surface for non-fouling pool boiling leads to higher heat transfer coefficients due to increased nucleation sites, increased turbulence, and lower fouling [6], [17], [31]. One reason for this discrepancy could be because the adhesion strength at rougher surfaces is higher, requiring more stress to remove fouling, and therefore the fouling layer is thicker as seen in Figure 3.5A leading to a lower heat transfer coefficient for the homogeneous $5\ \mu\text{m}$ and $10.5\ \mu\text{m}$ microchannel tests.

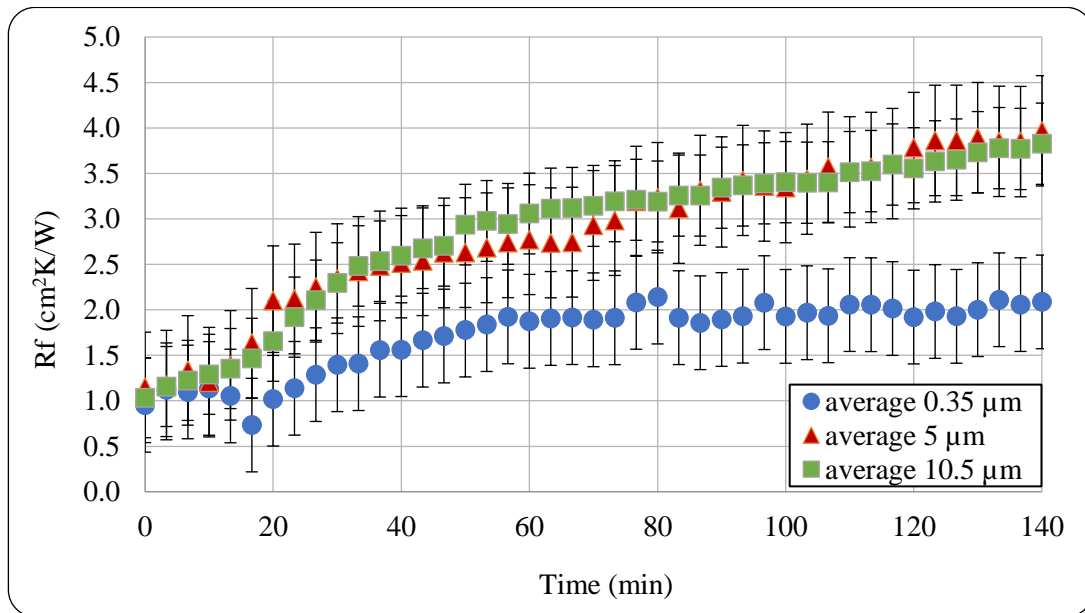


Figure 3.5A Impact of surface roughness on fouling resistance

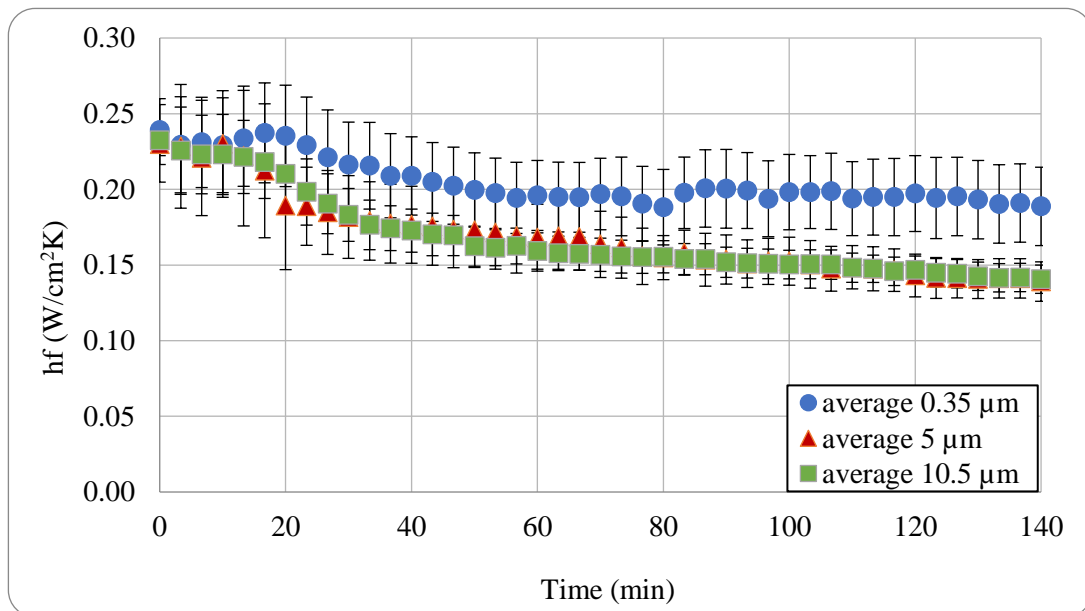


Figure 3.5B Impact of surface roughness on heat transfer coefficient

3.4.3. Effect of ethylene glycol on fouling

After all surface roughness tests were completed, the heterogeneous 10.5 μm surface with microchannels tests was repeated with an additional 3% ethylene glycol (EG) by mass to

determine if an organic compound would influence the fouling resistance or heat transfer coefficient. EG was chosen as it is used to produce in many antifouling surface coatings and is present in oil and gas wastewater. Figure 3.6 shows the fouling resistance and heat transfer coefficient results discussed previously with the addition of the 10.5 μm microchannel surface roughness with 3% EG included in the solution. The test with ethylene glycol had no identifiable effect on the fouling resistance or heat transfer coefficient compared to the 10.5 μm test with saline water. Therefore, adding ethylene glycol to a high-salinity solution does not affect the fouling resistance.

Figure 3.7 shows example pictures of the aluminum surface after a 140-minute test for the 3 surface roughness conditions and the test with 3% EG. These pictures further emphasize that the homogeneous 0.35 μm surface had less fouling accumulation than the other tests as it has the least amount of visible fouling and unfouled surfaces can be seen.

In the 0.35 μm picture, at the top of the aluminum there is a section which is completely fouled which corresponds with the water level during the test. This indicates that the water-steam interface may have a high impact on fouling accumulation as the liquid vapor interface has the fastest rate of salts separating and thus results in the highest quantity of fouling deposits. In the other three pictures (5 μm , 10.5 μm , and 10.5 μm with 3% EG) the surface is covered with salt accumulation and there is no noticeable difference between the fouling for the different tests. These pictures are consistent with the measured data for both the fouling resistance and heat transfer coefficient. In the 10.5 μm microchannel tests with and without the EG the fouling has begun fill and cover the grooves that were on the surface, changing the surface roughness as more salt accumulates and reducing the impact of the microchannels used in boiling systems.

3% EG was chosen for this work as it is estimated to be present in hydraulic fracturing wastewater which could be purified in a desalination system. Understanding the impact of EG on fouling will change the required operation and maintenance of purifying hydraulic fracturing wastewater [28]. If the concentration of EG was increased and began to affect the solubility or crystal structure of deposits, we would expect a change in fouling and further work should be done to understand the concentrations where EG may impact fouling resistance. Therefore, desalination plants should not be concerned regarding changes in fouling due to increased ethylene glycol levels. Further research should be done to determine if other organic compounds have an impact on fouling and if so, which organic compounds

will increase fouling as these will increase maintenance and operation costs. Understanding how fouling reacts with different chemicals present will help expand what mixtures can be treated using common desalination technologies.

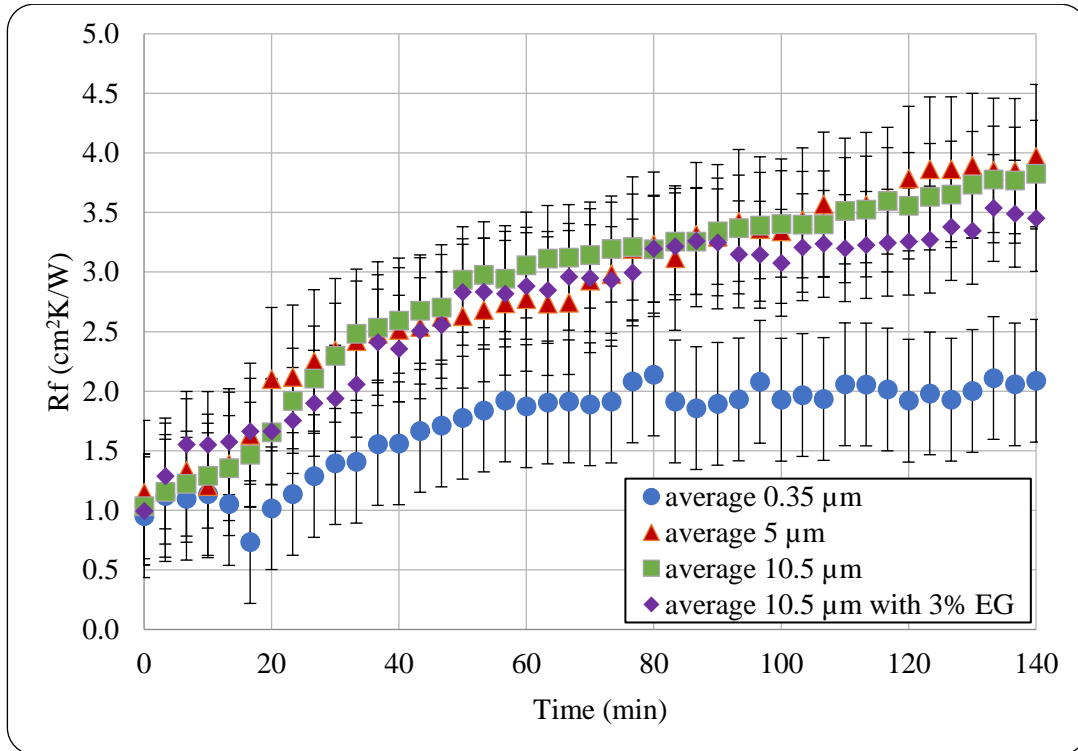


Figure 3.6A Impact of surface roughness and ethylene glycol (EG) on fouling resistance

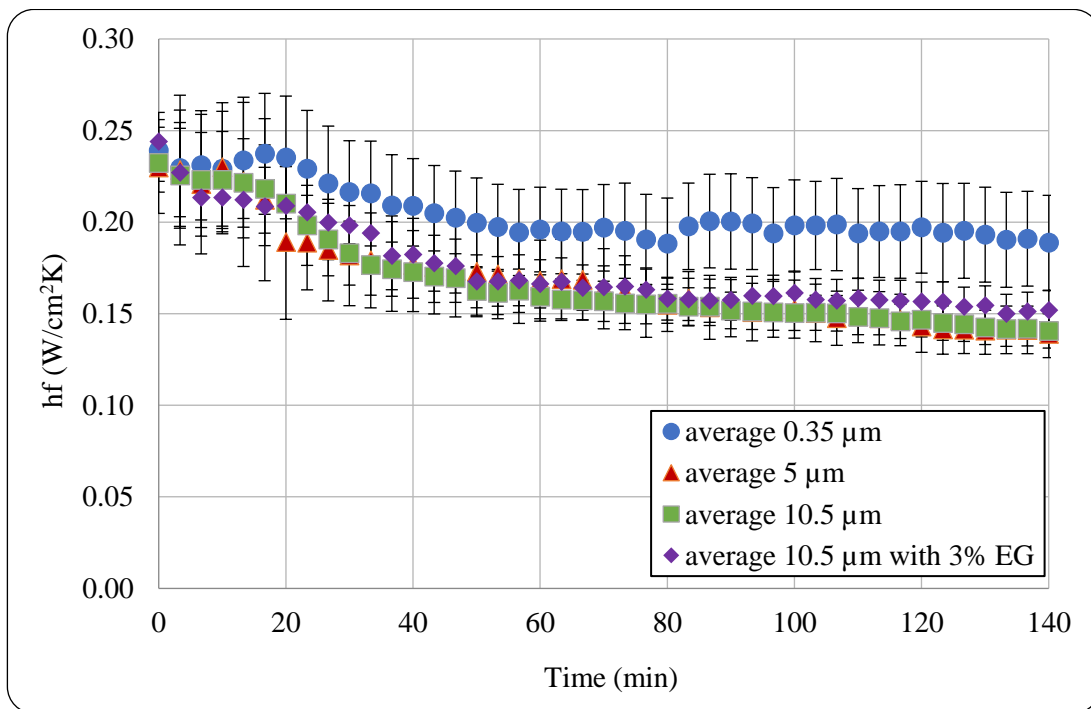


Figure 3.6B Impact of surface roughness and ethylene glycol (EG) on heat transfer coefficient

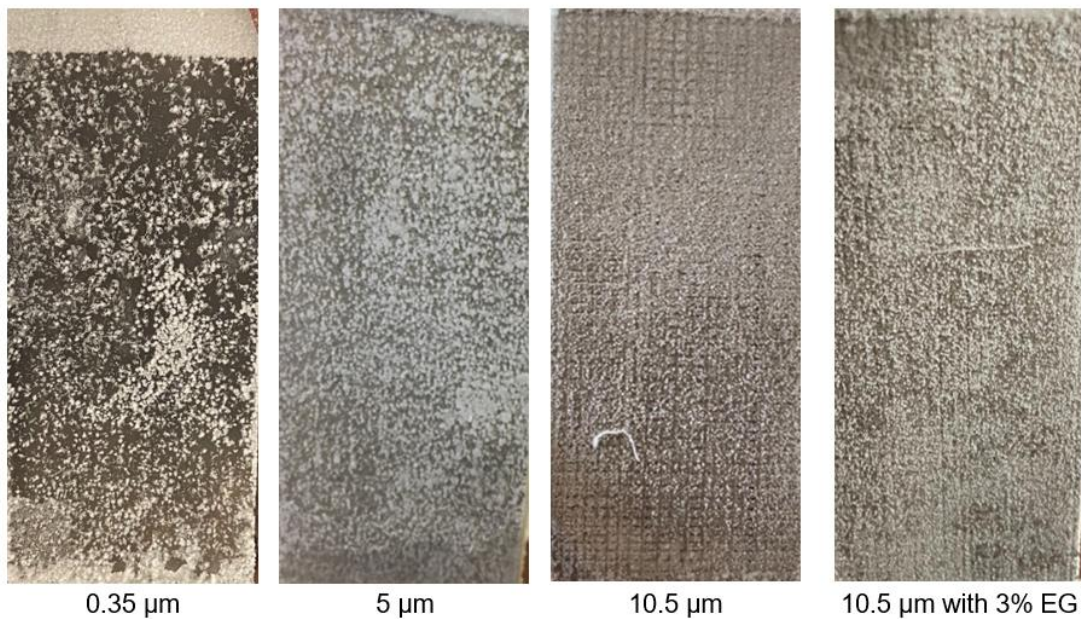


Figure 3.7 Example pictures of crystallization fouling for average roughness of 0.35 μm , 5 μm , 10.5 μm microchannel, and 10.5 μm microchannel with 3% ethylene glycol in the solution after 140 minutes

3.4.4. Effect ethylene glycol on salt composition

While there was no discernable difference in the fouling resistance with the presence of ethylene glycol, the salts that adhered to the aluminum surface were chemically different. Figure 3.8 shows the different elements that accumulated on the heat exchange surface with and without the 3% EG in the solution. These results were obtained from an ICP-OES analysis. Magnesium, potassium, calcium, and sulfur elements can each be attributed to one salt dissociating (magnesium chloride, sodium sulfate, calcium chloride, and potassium chloride), however the sodium elements could come from either the sodium chloride or sodium sulfate as both have sodium ions. With no EG present there is significantly more sodium ions that contributed to fouling than with 3% EG. With 3% EG there is a reduction of sodium ions and an increase in calcium and sulfate ions. While there was no change in the overall fouling resistance with or without EG present, it has affected which salts are attributing to crystallization fouling. Therefore, adding EG into a solution could be useful to reduce specific salts from fouling if specific salts have higher adhesion or unattractive qualities. For example, this work shows adding EG reduces salts containing sodium ions from adhering to the heat exchanger surface. Despite a large percentage of magnesium chloride in the original solution (26.5% of the initial salts) only very small amounts of magnesium and potassium ions are contributing to fouling with or without the presence of 3% EG indicating they are unlikely to cause fouling in a boiling system. Adding 3% EG had minimal effects on magnesium and potassium, but it did increase the presence of calcium and sulfate ions.

In tests with and without EG sodium ions were the largest attributers to crystallization fouling. This suggests that salts with sodium ions must be carefully managed to avoid fouling accumulation. As there were less sodium ions present in the salts collected from the EG test, one solution could be to add an organic compound such as EG; however, as discussed previously, changing the elements that adhered to the heat exchange surface did not change the overall fouling resistance. Further research should be done to understand how concentration and type of organic compound affects the salts that adhere to heat exchange surfaces.

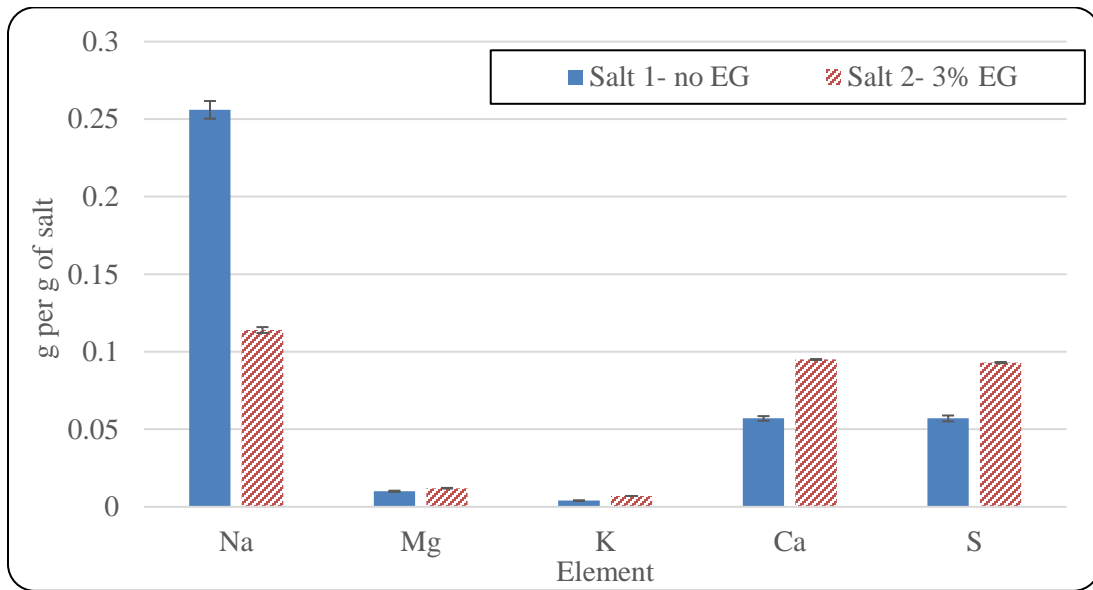


Figure 3.8. ICP-OES data showing the elements that accumulated on the aluminum block's surface for a microchannel 10.5 μm average surface roughness with (Salt 2) and without (Salt 1) 3% ethylene glycol present in the solution

3.5. Conclusion

Prior to this study fouling characteristics had been studied for specific situations such as low salinities (that of seawater or less), subcooled boiling systems, and single salt solutions but little research had been done to characterize fouling for high-salinity multiple salt solutions in a pool boiling regime. This study adds to the existing literature by determining the fouling resistance and heat transfer coefficient as mixed salts accumulate on a heat exchange surface with different surface roughness in a high-salinity pool boiling environment. Understanding how surface roughness affects fouling accumulation is important to improving treatment for desalination brine discharge with high salinity and multiple salts to increase treatment efficiency and reduce operation costs. This study determined the effect of 0.35 μm , 5 μm , 10.5 μm (microchannel) surface roughness on a 20% salinity solution made up of the most prevalent five salts found in natural sea water (sodium chloride, magnesium chloride, sodium sulfate, calcium chloride, potassium chloride) to mimic seawater desalination brine discharge.

- Fouling resistance does not increase as aluminum surface roughness increases from 5 - 10.5 μm , however lowering the surface roughness to 0.35 μm does decrease the fouling resistance by 1.5 cm^2/W . Therefore, it can be concluded that surface roughness is not the dominant parameter in fouling accumulation for aluminum with

an average surface roughness between 5 μm and 10 μm for the tested conditions but does have an impact between 5 μm and 0.35 μm .

- The fouling resistance associated with homogeneous 5 μm and 10.5 μm microchannel average surface roughness increases linearly with time after the initialization period indicating the fouling is resilient and has strong adhesion to the surface and it would be inaccurate to assume a constant fouling resistance during modeling.
- Fouling resistance with 0.35 μm surface roughness increased for the first 60 minutes of the 140-minute test before plateauing at 2 $\text{cm}^2\text{K/W}$ indicating that the fouling is asymptotic and the deposit removal due to shear stress from boiling and the fouling accumulation is equal. It also indicates a constant fouling resistance value can be used to model a heating surface with 0.35 μm surface roughness during pool boiling.
- During tests with 3% ethylene glycol, an organic compound used to make antifouling coatings, there was no change in fouling behavior observed compared to tests with no ethylene glycol. This indicates that solutions containing ethylene glycol should not be a concern with regards to crystallization fouling in desalination systems and will provide no benefit in fouling prevention if EG is mixed with the solution unless utilized with other mitigation techniques to selectively choose which salts adhere to the surface.

Further research is needed to better understand how the geometry of the heating system may play a role in fouling accumulation, how adding other organic compounds may impact fouling, and what other factors dominate fouling accumulation when surface roughness is sufficiently smooth ($< 0.35 \mu\text{m}$). We are currently working on extensive boiling flow tests with the same mixture of salts to compare the effect of flow and orientation on fouling which will be presented in a future publication. The results from this paper will help improve heat exchange surface design for use in desalination systems to allow for higher freshwater yield and a reduction in environmentally damaging brine waste.

Declaration of competing interest

The authors declare that they have no known competing financial interests or personal relationships that could have appeared to influence the work reported in this paper.

Acknowledgements

This work is supported by the US Department of Energy, Advanced Research Projects Agency – Energy (ARPA-E) award number DE-AR-0001000. Results of this work do not

necessarily reflect the views of the Department of Energy. The authors acknowledge the support from Kathy Hu and Elnaz Nikooei at Oregon State University in Corvallis, OR for their contributions in experimental design and analysis

Author contributions

Morgan Messer and Kyle Anderson prepared the experimental setup and conducted experiments including collecting and processing data. Morgan Messer, Kyle Anderson, and Bahman Abbasi formulated the paper. All authors conceived the study, approved the final version of the manuscript, and agree to be held accountable for content therein.

Nomenclature

R_a	Arithmetic average of roughness profile
R_f	Fouling resistance
h_f	Heat transfer coefficient after fouling
h_0	Initial heat transfer coefficient
q''	Heat flux
$T_{s,f}$	Temperature of surface after fouling
$T_{s,0}$	Initial temperature of surface
$T_{w,f}$	Temperature of water after fouling
$T_{w,0}$	Initial temperature of water
T_s	Block surface temperature
$T_{TC,o}$	Outer thermocouple temperature
$T_{TC,i}$	Inner thermocouple temperature
$R_{al,o}$	Outer aluminum thermal resistance
$R_{al,i}$	Inner aluminum thermal resistance
$D_{al,o}$	Outer thermocouple to block surface length
D_{tp}	Thermal paste length
k_{al}	Thermal conductivity of aluminum

k_{tp}	Thermal conductivity of thermal paste
R_0	Reference resistance of RTD
$R(T)$	Resistance measured by RTD
T	Temperature measured by RTD
A	A coefficient in Callendar-Van Dusen equation
B	B coefficient in Callendar-Van Dusen equation

References

- [1] United Nations, "Summary Progress Update 2021: SDG 6 — water and sanitation for all," 24 February 2021. [\[Online\]](#).
- [2] D. Rubio, C. López-Galindo, J. F. Casanueva and E. Nebot, "Monitoring and assessment of an industrial antifouling treatment. Seasonal effects and influence of water velocity in an open once-through seawater cooling system," *Applied Thermal Engineering*, vol. 67, no. 1-2, pp. 378-387, 2014.
- [3] Helalizadeh, H. Müller-Steinhagen and M. Jami, "Mixed salt crystallization fouling," *Chemical Engineering and Processing*, vol. 39, pp. 29-43, 2000.
- [4] S. Kazi, K. Teng, M. Zakaria, E. Sadeghinezhad and M. Bakar, "Study of mineral fouling mitigation on heat exchanger surface," *Desalination*, vol. 367, pp. 248-254, 2015.
- [5] P. A. Raghupathi and S. G. Kandlikar, "Characterization of Pool Boiling of Seawater and Regulation of Crystallization Fouling by Physical Aberration," *Heat Transfer Engineering*, vol. 38, pp. 1296-1304, 2017.
- [6] S. N. Kazi, "Fouling and Fouling Mitigation on Heat Exchanger Surfaces," *Basic Design Applications*, 2012.
- [7] M. Jamialahmadi and H. Müller-Steinhagen, "Crystallization of Calcium Sulfate Dihydrate from Phosphoric Acid," *Developments in Chemical Engineering Mineral Processing*, vol. 8, no. 5-6, pp. 587-604, 2000.
- [8] Janzen and E. Y. Kenig, "Analysis of crystallization fouling in electric water heating," *Heliyon*, vol. 5, no. 11, 2019.
- [9] Helalizadeh, H. Müller-Steinhagen and M. Jami, "Mathematical modelling of mixed salt precipitation during convective heat transfer and sub-cooled flow boiling," *Chemical Engineering Science*, vol. 60, pp. 5078-5088, 2005.
- [10] Panagopoulos, M. Loizidou and K. J. Haralambous, "Desalination Brine Disposal Methods and Treatment Technologies A Review," *Science of the Total Environment*, vol. 693, 2019.
- [11] Janzen and E. Kenig, "Understanding and Analysis of Fouling Behavior on bare-wire heating elements in electric water heating," *Heat Exchanger Fouling and Cleaning*, 2019.

- [12] S. M. Peyghambarzadeh, A. Vatani and M. Jamialahma, "Application of asymptotic model for the prediction of fouling rate of calcium sulfate under subcooled flow boiling," *Applied Thermal Science*, vol. 39, pp. 105-113, 2012.
- [13] K. Song, J. Lim, S. Yun, D. Kim, Y. Kim, "Composite fouling characteristics of CaCO₃ and CaSO₄ in plate heat exchangers at various operating and geometric conditions," *International Journal of Heat and Mass Transfer*, vol. 136, pp 555-562, 2019
- [14] J. MacAdam and S. A. Parsons, "Calcium carbonate scale formation and control," *Reviews in Environmental Science and Bio/Technology*, vol. 3, pp. 159-169, 2004.
- [15] S. Keysar, R. Semiat, D. Hasson and J. Yahalom, "Effect of Surface Roughness on the Morphology of Calcite Crystallizing on Mild Steel," *Journal of colloid and interface science*, vol. 162, pp. 311-319, 1994.
- [16] Y. Liu, Y. Zou, L. Zhao, W. Liu and L. Cheng, "Investigation of adhesion of CaCO₃ crystalline fouling on stainless steel surfaces with different roughness," *International Communications in Heat and Mass Transfer*, vol. 38, pp. 730-733, 2011.
- [17] F. Albert, W. Augustin and S. Scholl, "Roughness and constriction effects on heat transfer in crystallization fouling," *Chemical Engineering Science*, vol. 66, pp. 499-509, 2010.
- [18] J. S. Kim, A. Girard, S. Jun, J. Lee and S. M. You, "Effect of surface roughness on pool boiling heat transfer of water on hydrophobic surfaces," *International Journal of Heat and Mass Transfer*, vol. 118, pp. 802-811, 2018.
- [19] J. Jones, J. P. McHale and S. V. Garimella, "The Influence of Surface Roughness on Nucleate Pool Boiling Heat Transfer," *Journal of Heat Transfer*, vol. 131, 2009.
- [20] A. Warlo, B. Nienborg, H. Fugmann, M. Altenberend, L. Schnabel, K. Conzelmann, M. Mathieu and A. Schwärzler, "Experimental Characterization of Fouling in Context of Heat Exchanger Development," *Heat Exchanger Fouling and Cleaning*, 2019.
- [21] J. S. Kim, A. Girard, S. Jun, J. Lee and S. M. You, "Effect of surface roughness on pool boiling heat transfer of water on hydrophobic surfaces," *International Journal of Heat and Mass Transfer*, vol. 118, 2017.
- [22] M. Jamialahmadi and H. Müller-Steinhagen, "A New Model for the Effect of Calcium Sulfate Scale Formation on Pool Boiling Heat Transfer," *Journal of Heat transfer*, vol. 126, pp. 507-517, 2004.
- [23] T. Ekblad, G. Bergström, T. Ederth, S. L. Conlan, R. Mutton, A. S. Clare, S. Wang, Y. Liu, Q. Zhao, F. D'Souza, G. T. Donnelly, P. R. Willemsen, M. E. Pettitt, M. E. Callow, J. A. Callow and B. Liedberg, "Poly(ethylene glycol)-Containing Hydrogel Surfaces for Antifouling Applications in Marine and Freshwater Environments," *Biomacromolecules*, vol. 9, no. 10, pp. 2775-2783, 2008.
- [24] Banerjee, R. C. Pangule and R. S. Kane, "Antifouling Coatings: Recent Developments in the Design of Surfaces that Prevent Fouling by Proteins, Bacteria, and Marine Organisms," *Advanced Materials*, vol. 23, no. 6, pp. 690-718, 2010.
- [25] E. M. Van Wagner, A. C. Sagle, M. M. Sharma, Y. H. La and B. D. Freeman, "Surface modification of commercial polyamide desalination membranes using poly(ethylene glycol) diglycidyl ether to enhance membrane fouling resistance," *Journal of Membrane Science*, vol. 367, pp. 273-287, 2011.
- [26] A. L. Truschel, "What Is Polyethylene Glycol?," *Sciencing*, April 2017. [\[Online\]](#).

- [27] Abbasi, X. Zhang, H. O'Hern and E. Nikooei, "Method and System for Purifying Contaminated Water". United States Patent 62882970, 4 August 2020.
- [28] H. O'Hern, E. Nikooei, X. Zhang, C. Hagen, N. AuYeung, D. Tew and B. Abbasi, "Reducing the water intensity of hydraulic fracturing: a review of treatment technologies," *Desalination Water Treatment*, vol. 221, pp. 121-138, 2021.
- [29] E. Nikooei, N. AuYeung, X. Zhang, K. Goulas and B. Abbasi, "Controlled dehumidification to extract clean water from a multicomponent gaseous mixture of organic contaminants," *Journal of Water Process Engineering*, vol. 43, 2021.
- [30] "Sea Salt ASTM D1141-98," ASTM Synthetic Seawater, [\[Online\]](#).
- [31] M. Haghshenasfard, G. H. Yeoh, M. Dahari and K. Ho, "On numerical study of calcium sulphate fouling under sub-cooled flow boiling conditions," *Applied Thermal Engineering*, vol. 81, pp. 18-27, 2015.

CHAPTER 4: Crystallization fouling management in hypersaline flow boiling

Morgan Messer¹, Katerina Reynolds¹, Bahman Abbasi^{1*}

Oregon State University, 1500 SW Jefferson Way, Corvallis, OR 97331, USA

*Corresponding author: AbbasiB@oregonstate.edu

Crystallization fouling management in hypersaline flow boiling

Abstract

With fresh water supplies diminishing and demand for water increasing worldwide, desalination is one possible method to increase water supplies by treating saline water. Managing crystallization fouling while humidifying or evaporating saline water in a humidification dehumidification desalination system is a challenge. An electrically heated aluminum pan with baffles to control flow path and velocity was utilized to identify operating parameters for mitigating fouling in a 10% sodium chloride and 10% potassium chloride saline solution. The inlet flow rate was varied from 2.3-3.1 g/s with input power of 3,730 W. For inlet flow rates of 2.3-2.8 g/s, fouling occurred within the first 30 minutes of testing causing blockages when the water evaporation rate was 73% requiring additional fouling mitigation techniques to continue operation. For inlet flow rates between 2.9-3.1 g/s, no fouling occurred in the system after 4 hours of steady state operation with a water evaporation rate of 52-54%. Crystallization fouling in this environment is very loose and could be removed with targeted flushing. Flushing the last column, where fouling occurred, during 2.3-2.8 g/s inlet flow rate tests removed the majority of the fouling and had no impact on the overall evaporation rate as the overall system disturbance was minimized.

Keywords: Evaporation, Fouling mitigation, Saline, Desalination

4.1. Introduction

Fresh water supplies are diminishing around the globe. For example, about half of European countries are facing water shortages, the United States is consuming freshwater faster than it can be replenished, Egypt imports half of their food supply due to lack of water, and 550 of China's 600 largest cities have a water deficient [1]. As the demand for water continues to increase, the demand for water purification technologies does as well. Desalination is one of many technologies aimed to increase water supply by treating saline water, however, it does have its challenges.

Crystallization fouling, or fouling caused by inorganic materials (salts) adhering to a surface thereby reducing heat transfer and causing blockages, is the most common fouling that occurs in desalination systems as seawater is 70% inorganic [2]. Crystallization fouling is influenced by many different parameters such as momentum, heat and mass transfer, chemical kinetics, surface roughness, solution pH, salt type, surface material, salt concentration, surface temperature, etc. [3]. These many parameters make it difficult to predict the quantity, the location of fouling, or completely avoid fouling. Fouling mitigation takes many forms, but it must be specific to the system and optimized. Common fouling mitigation techniques include controlling flow velocity, periodic cleaning, surface coatings, changing surface roughness, adding chemicals, or introducing physical methods such as vibration or ultrasonic. Various studies on these methods are reported in the literature [4], [5]. It is important to understand the application of different methods in each real-world system.

4.1.1. Boiling

Boiling has several effects on fouling accumulation as salt deposits can temporarily increase the number of nucleation sites in the system, which can temporarily increase heat transfer [3], [6], [7]. As boiling removes water from a saline solution, salinity increases, which increases fouling as fouling is highly dependent on the degree of supersaturation [6], [8]. While most desalination plants concentrate on low salinity (1-3.5%), it is important to determine the effect of high salinity (over 5% and even above 20%) and how to manage fouling at high salinities to effectively treat and boil brine wastewater [1]. In addition, as bubbles form on the heated surface, local supersaturation occurs, which can result in salt deposits even when the salinity of the overall solution is below the salt saturation point causing fouling accumulation to accelerate [9]. Two pool boiling studies done with saline water found increased critical heat flux (CHF) due to increased nucleation site density, bubble departure diameter increases, increased thermal resistance, and a change in the heat transfer coefficient [10], [11]. Understanding how to mitigate fouling in a highly saline boiling environment is important to effectively design and treat high salinity desalination systems. The goal is to minimize the liquid layer thickness to maximize the local heat transfer coefficient but avoid local supersaturation and dryouts that can calcify salt deposits and greatly reduce heat transfer.

4.1.2. Flushing

Periodic cleaning is required to remove fouling and blockages in desalination systems regardless of the type of fouling mitigation techniques implemented. Two popular cleaning methods for removing fouling involves backwashing a fluid through the system or air sparging, which involves injecting air into the system both disrupt fouling and increase turbulence [4]. These methods are effective and commonly used in desalination systems. They are done during system operation with minimal impact to the overall system while still managing fouling. A study by Xia et al. [12] found that unsteady air sparging was more effective in eroding fouling deposits in membrane desalination than constant flow flushing as an unsteady flow increased system turbulence. Utilizing water instead of air in the forward flow direction minimizes discontinuity in the system. Flushing the system with water increases solution velocity, which increases turbulence and shear stress. This can decrease fouling and remove fouling deposits. In addition, increasing velocity can alter fouling deposition from being a mass-controlled system to being a chemically controlled system [8]. By combining these two methods of air sparging with water backwashing it could help manage fouling in a thermal desalination system more effectively than a single method.

4.1.3. System design

A research team at Oregon State University is developing a new desalination system to treat hydraulically fractured wastewater (water with high (> 20%) salinity and multiple contaminants) using a humidification dehumidification (HDH) system [12]. The system involves utilizing a heating unit to partially boil the contaminated water stream. This removes contaminants that have a higher boiling point than water. Downstream, contaminants with lower boiling points than water will be removed through the condensation process [14]. The system requires an evaporation zone be designed to effectively control evaporation rate and temperature to reduce contaminants that evaporate with the water. The evaporation zone must be able mitigate crystallization fouling in a highly saline environment. As the system is designed to treat high salinity wastewater (20% and higher), well above the salinity for most desalination treatment plants (1-3.5%), it is critical for this system design to manage fouling appropriately to maintain energy efficiency and reduce required system maintenance [1]. This system was the motivation behind this study.

4.1.4. This study

Crystallization fouling mitigation is difficult to implement using one singular method as fouling is impacted by many different parameters. It is important to understand these parameters and test how various methods work when applied to a system. While fouling during boiling processes has been studied to determine the influence of different parameters, few studies have been done with highly saline solutions ($> 3.5\%$), which are more representative of brine solutions that are not commonly treated with traditional desalination technologies. Therefore, this study was designed to understand the operational points in a system with bottom heating for a 20% saline solution where flow is controlled both in terms of residence time and flow path. The objective was to minimize fouling and determine the maximum possible evaporation rate before fouling would inhibit the system operation lower efficiency and filling with salt. To do this a simple model was developed to help target fouling mitigation techniques that correspond to different areas of the pan (before and after salt saturation). Several tests were done with varying input flow rates to determine the water evaporation rate at which fouling could be managed more easily and at what flow rates fouling obstructed the flow leading to excessive fouling and increased fouling resistance. In addition, tests were done with targeted water flushing to demonstrate how this technique could be used in combination with flow rate and power control in a location where the system was saturated and fouling. The objective was to mitigate fouling with minimal system disruption and loss of water production.

4.2. Experimental setup

Figure 4.1 A and B show the experimental setup used in this study. An aluminum pan (3) is heated by four electrically heated plates (13.2 cm by 13.3 cm) spaced to provide constant, even heating. Aluminum was chosen as it is easy to work with, has a desirable heat transfer coefficient, and does not corrode. Heat transfer putty (TRACIT-600A) was used to eliminate any air gaps between heaters and the aluminum pan. The pan was clamped to the stand to keep it from deforming or moving between testing, ensure good contact with the heaters and hold the polycarbonate lid (8) to the pan as shown in Figure 4.1 B. Heaters were positioned about 1.3 cm apart and from the outside of the pan as shown in Figure 4.1 D, a CAD with a transparent bottom to show the location of the heaters. Superwool Plus MD paper insulation was used between heaters and the heating stand to reduce surrounding heat loss. Each

electrical heater was individually controlled using a Belee 20 A variable voltage transformer and monitored with a Baldr power meter (4). Power was kept constant throughout each test and reordered periodically. Aluminum pan dimensions are 310 mm x 310 mm x 50 mm with a 25 mm x 50 mm extension near the discharge, as shown in Figure 4.1 D, to allow adequate room for a vertical 1.3 cm discharge that sits flush with the inside of the pan. There are 5 mm aluminum baffles inside the aluminum pan to create one wide (54 mm) pass and nine narrower (25 mm) passes to control the flow path of the saline mixture. The path of the saline mixture is shown in by the arrows in Figure 4.1 B. Baffles control the length of the flow path and the residence time. The wider initial path allows the saline mixture to flow at a slower velocity while it sensibly heats without risk of fouling. The flow path was narrowed after it was predicted to reach boiling to achieve a higher velocity with less stagnation to avoid fouling accumulation. As velocity increases, the risk of fouling resistance decreases due to increased turbulence and shear stress that can remove deposits [15]. The flow path is curved to keep a consistent size and eliminate sharp turns where stagnation would occur in the corners.

The saline mixture was continuously pumped into a 6 mm tube on the left side of the pan using a Masterflex L/S displacement pump (2) to control the flow rate during testing. Inlet water temperature was measured with a Type K thermocouple and recorded periodically to ensure constant water temperature (1). The unevaporated mixture exits the pan through the vertical discharge port where it flows into a container (6) on a Dymo M10 scale (7) that records weight every 0.5 seconds to measure the discharge rate. Some tests utilized a 6 mm thick clear polycarbonate lid (8) lined with gasket material to create a seal during testing and allow vapor to escape through a 33 mm hole in the lid.

Figure 4.1 B shows a small 0.6 cm port located on the last turn of the flow path and is angled at 45° referred to as the flush inlet. This tube was used in conjunction with a Kamoer DIPump550 displacement pump (5) to test how different flow rates and times could be used to flush any accumulated salt blocking the discharge during fouling mitigation testing.

The inlet mixture was 10% sodium chloride (NaCl) and 10% potassium chloride (KCl) for 20% total salinity. Sodium chloride and potassium chloride were chosen as these salts are common in nature and are commonly found in hydraulic fracturing wastewater [12]. Saline water was made by mixing potassium chloride and sodium chloride with water using a magnetic stir plate for 30 minutes. It was preheated using a hotplate before being pumped

into the pan via the Masterflex displacement pump (2). The pan was cleaned between tests by scrubbing away any salts that were in the system and rinsing with pure water.

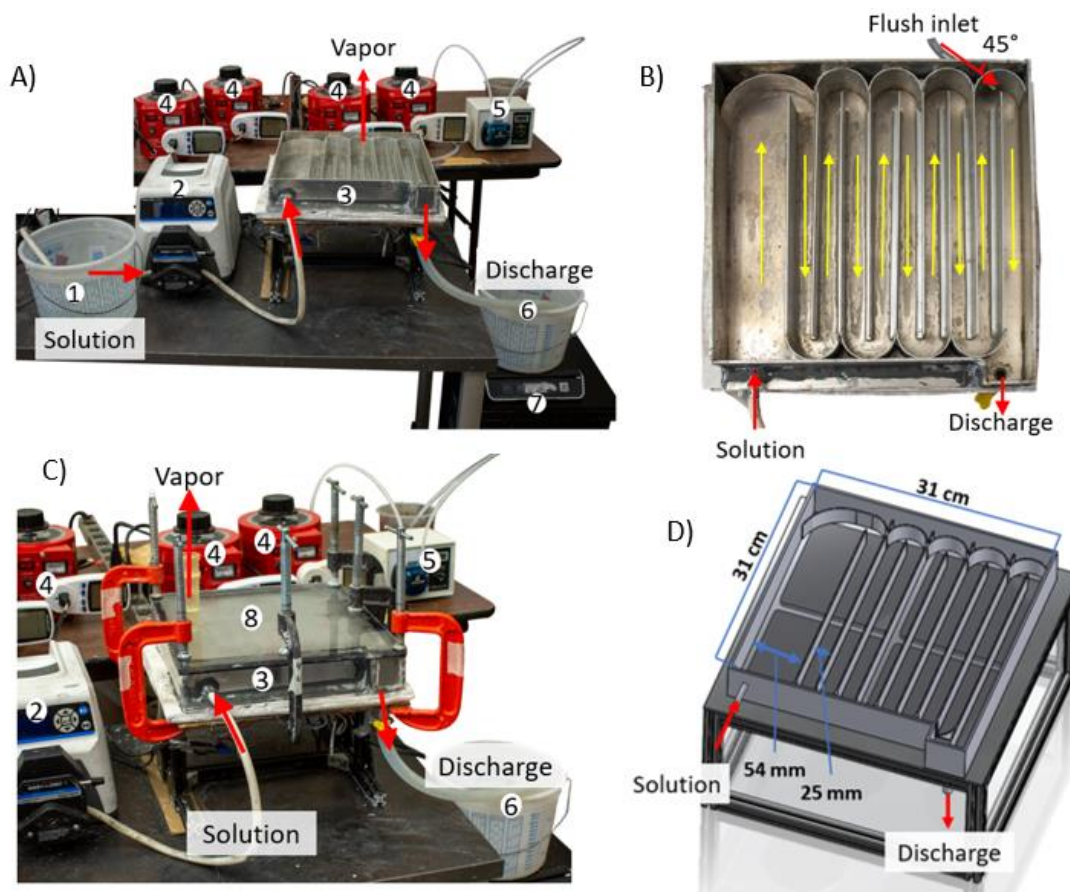


Figure 4.1 Experimental setup of a bottom heated evaporation system A) full experimental setup, B) close up of the evaporation pan and the flush inlet location, C) experimental setup with a polycarbonate lid, D) CAD diagram of evaporation pan showcasing the 4 heater's positions. (1) preheated mixed solution, (2) Masterflex L/S displacement pump, (3) Aluminum evaporation pan, (4) Belee 20 A variable voltage transformer Baldr power meter, (5) DIPump550 displacement pump, (6) discharge container, (7) Dymo M10 scale, (8) polycarbonate lid with vapor outlet

4.3. Methodology

The following methodology was used to determine the percent of water evaporation, heating efficiency, and energy consumption of the evaporation zone. Eq. 1 was used to determine the heating efficiency of the system.

$$\eta_{heating} = \frac{\dot{Q}_{sensible} + \dot{Q}_{latent}}{P} \quad (1)$$

$\dot{Q}_{sensible}$ is the sensible heating utilized for heating the inlet solution stream as calculated by Eq. 2 \dot{Q}_{latent} is the latent heating utilized in the water evaporation as calculated by Eq. 3. P is the power measured from the four heaters in the system.

$$\dot{Q}_{sensible} = \dot{m}_{solution} C p_{solution} (T_{boil} - T_i) \quad (2)$$

$$\dot{Q}_{latent} = \dot{m}_{evaporation} h_{fg_{solution}} \quad (3)$$

In Eq. 2 and 3, $\dot{m}_{solution}$ is the inlet flow rate of the saline solution, T_{boil} is the boiling temperature as measured by a thermocouple in the aluminum pan, T_i is the measured inlet solution temperature, $C p_{solution}$ is the weighted average of specific heats in the solution as shown in Eq. 4, $\dot{m}_{evaporation}$ is calculated as the difference between the inlet flow rate and the measured discharge flow rate during testing, and $h_{fg_{solution}}$ is the latent heat of vaporization as calculated in Eq. 5 [16], [17].

$$C p_{solution} = \left(\frac{m_{NaCl}}{m_{solution}} \right) C p_{NaCl} + \left(\frac{m_{KCl}}{m_{solution}} \right) C p_{KCl} + \left(\frac{m_{H_2O}}{m_{solution}} \right) C p_{H_2O} \quad (4)$$

$$h_{fg_{solution}} = (1 - s) h_{fg_{H_2O}} \quad (5)$$

In Eq. 4 and 5, m is the respective mass of each compound or the total mass of the solution, $C p$ is the respective specific heat of each compound, S (wt%) is the salinity as calculated by mass of salt over total mass of solution, $h_{fg_{H_2O}}$ is the latent heat of vaporization of water.

Lastly, the energy consumption is estimated as the ratio of power utilized to the amount of produced water using Eq. 6. The percentage of water evaporated compared to the initial amount of water was calculated using Eq. 7.

$$Energy\ consumption = \frac{P}{\dot{m}_{evaporation}} \rho_{H_2O} t \quad (6)$$

$$\%_{water\ evaporated} = \frac{\dot{m}_{evaporation}}{\dot{m}_{solution}(1 - s)} \quad (7)$$

In Eq. 6 and 7, ρ_{H_2O} is the density of water and t is the test duration.

The overall methodology assumes that the sensible energy of the unevaporated mixture is recuperated in the system, which is true if the discharge is moved back into the starting tank

where it is pumped into the evaporation zone to remove most of the contaminants or if there is a heat exchanger to recuperate some of the energy. It also assumes that $C_{p_{solution}}$ and $h_{fg_{solution}}$ are constant throughout the test and regardless of the location of the pan. These assumptions were considered acceptable for these tests as discharged mass was compared with the inlet conditions and efficiency in specific parts of the pan was not a concern.

4.3.1. Uncertainty analysis

Kline-McClintock and higher-order methods provided uncertainties along with their propagations [18]. Table 4.1 shows the final uncertainties for the calculated values which includes both instrument and precision uncertainty.

Table 4.1 Uncertainty in parameters for tests performed on the evaporation system

Parameters	Range	Uncertainty		Arithmetic mean
		Maximum	Minimum	
Inlet flow rate (g/s)	2.3 – 3.1	0.04	0.01	0.026
Inlet solution temperature (°C)	40 – 49	2	2	2
Power (W)	3633 – 3811	77	111	89
Evaporation rate (g/s)	1.22 – 1.6	0.01	0.07	0.04
Energy consumption (kWh/m ³)	652 - 845	15	54	32

4.4. Oversaturation location model to inform fouling mitigation strategies

Python was used to create a model that predicted local evaporation and salt oversaturation points. Rather than testing flow rate, heater power, and salinity variables through trial and error, the code provided insight into the testing methodology to determine fouling mitigation techniques. One of the ways to reduce fouling and maintain evaporation was to increase the time spent in the region between boiling and salt saturation locations. Decreasing the distance traveled by a saturated salt solution post boiling reduces the likelihood of supersaturation and thus fouling but evaporation should be maximized. The code estimated the boiling and salt saturation locations with respect to various inputs: inlet flow rate, inlet temperature, total heating power, heating efficiency, and salinity/salts utilized. When the salt saturation point was reached, the result dictated where to focus fouling mitigation strategies during experiments. The effect of baffle locations and quantities on fouling could also be estimated.

The larger entry area increases the residence time in the initial pass, which allows the solution to have more time to sensibly heat as the perimeter around the pan (13 mm from the edges) does not directly interface with the heaters. The wide channel also minimizes oscillations from the peristaltic pump and stabilizes fluid flow. The decrease in channel width afterwards increased the rate of fluid flow thereby increasing heat transfer and reducing fouling risk.

Outputs included the location in the pan at which the solution boiled, maximum salinity and its location, and the total evaporation rate as the solution flowed through the baffles. An average of the solution's path throughout the pan was used. Eq. 8 and 9 were used for determining density.

$$\rho_m = \frac{1}{w_{H_2O} \bar{v}_{H_2O} + \sum_i w_i \bar{v}_{app,i}} \quad (8)$$

$$\bar{v}_{app,i} = \frac{w_i + c_2 + c_3 t}{(c_0 w_i + c_1) e^{(0.000001(t+c_4)^2)}} \quad (9)$$

In Eq. 8 and 9, the mass fraction of each constituent is denoted as w with the subscripts of H_2O and i indicating water or the constituent in question, respectively.

Using constants (C_0, C_1, C_2, C_3, C_4) found by Laliberte and Cooper [19] for both KCl and NaCl, the apparent specific volume, $\bar{v}_{app,i}$, was calculated. The boiling location was calculated by iterating over the total single-phase heat transfer area until the output temperature reached boiling. The pan's surface was treated as smooth. Critical heat flux calculations confirmed that the system was below the boiling crisis and exhibiting a steady state. Similarly, Eq. 3 was iterated to determine the location of saturation, assuming it would occur at a single point and the total evaporation rate was also recorded. The code did not include heat loss or thermal paste resistance between heaters and the pan, but their effects were accounted for with a heat loss percentage.

Visual representations of locations in question were marked on photos taken of the experiment. An example is shown in Figure 4.2. An uncertainty of ± 25.4 mm for the experimental locations was deemed appropriate due to the difficulty in determining the exact location and repeatability between tests as boiling is not consistent. The code locations carried an uncertainty of the step size, 1.5 mm. This was sufficient resolution to inform fouling mitigation techniques. The boiling location for both the experimental values and estimated analytical were similar (within 26.2 mm for the test shown in Figure 4.2) and

within measurement uncertainties; however, the location of fouling does differ more and when fouling occurred near the exit, code results indicated no fouling within the pan.

Figure 4.2 shows that the maximum salinity of the code was calculated to be 3065 mm compared to the experimental value of 2959 mm. In these cases, experimental fouling was attributable to local salt supersaturation whereas the code only accounted for the solution's salt saturation. Quantitative results showed comparability and reproducibility between these two methods, with percent differences not exceeding 2.5% for model and experimental comparisons. This code was used only to provide an estimate of boiling and fouling locations in the pan to inform fouling mitigation techniques and target specific areas (before boiling, before and after salt saturation).



Figure 4.2 Boiling and fouling locations of experiment and code estimates for 2.8 g/s 10% NaCl and 10% KCl saline

4.5. Results and discussion

4.5.1. Evaporation rate and cost of produced water

Table 4.2 provides an overview of experimental results relating to various flow rates (2.3-3.1 g/s) for the tested saline mixture 20% salinity consisting of 10% NaCl and 10% KCl. Results for each flow rate include their respective evaporation rates, percent water evaporation, time before fouling affected the flow or heat transfer, heating efficiency, and the cost of evaporated or produced water. The energy to sensibly heat water to account for the difference in inlet temperature is small (< 2%) between tests because vast majority of energy consumption is due to the latent heat of evaporation.

As the inlet flow rate increases, the percentage of evaporated water decreases from 85% at 2.3 g/s to about 53% at 2.8-3.1 g/s. This is expected as at 2.3 g/s there is much less overall water in the solution to evaporate with the same power input so more water can evaporate quicker. In addition, for water evaporation rates higher than 73%, fouling occurred quickly (within 15-30 min) after testing commenced, and this fouling obstructed the discharge outlet greatly reducing or eliminating the amount of saline water that could be discharged. This would be considered a critical failure in the system as it is not designed for salt to adhere to the surface or fully evaporate the feed stream as this would not separate contaminants. Fouling would continue forming thereby reducing heat transfer and requiring system maintenance. Increasing the inlet flow rate with 20% salinity water to achieve an evaporation rate of 53% or less has no significant fouling during the hour-long test, which avoids the need for constant cleaning and maintenance.

In addition, the test with 3.1 g/s at 20% salinity was tested for 4 hours with a 52% water evaporation rate with no fouling or any indication of fouling. This indicates that maintaining a 52% water evaporation rate with 20% inlet salinity in this system is sustainable for a longer duration and would not require other fouling mitigation techniques or maintenance during that time. It should be noted that with other flow path designs and residence time inside the pan, this value may differ slightly. The 3 g/s test had a 4-minute residence time with the current flow path/baffle setup (1 wide path followed by 9 narrower passes).

While the cost of produced water may be lower for 2.3-2.8 g/s tests (around 650-700 kWh/m³), it cannot operate for a long duration due to fouling. As previously pointed out, these flow rates are too low causing fouling to occur within 30 minutes of testing and only a minimal amount of water can be produced before the test reaches critical failure (no

discharge). Fouling mitigation or maintenance would be required adding to the cost of the produced water with much less overall production. Conversely, higher inlet saline water flow rates (2.9-3.1 g/s) achieved more reasonable results as it could operate with 52% water evaporation for 4 hours with no fouling and only slightly higher energy costs. In addition, if the cost of maintenance required for the lower (2.3-2.8 g/s) inlet flow rates was considered it may be more costly as it would need additional fouling mitigation techniques or cleanings much more frequently than the higher inlet flow rates that had no fouling.

Table 4.2 Evaporation and cost of produced water results for various 20% saline water flow rates (2.3-3.1 g/s)

Inlet flow rate (g/s)	Inlet temperature (°C)	Power (W)	Evaporation rate (g/s)	Percent of water evaporated	Time before fouling (minutes)	Heating efficiency	Energy consumption (kWh/m ³)
2.3 ± 0.03	44 ± 2	3811 ± 96	1.6 ± 0.03	85%	15 min	87%	675 ± 17
2.6 ± 0.03	49 ± 2	3780 ± 111	1.5 ± 0.04	73%	20 min	85%	703 ± 30
2.8 ± 0.01	47 ± 2	3781 ± 83	1.6 ± 0.01	73%	30 min	91%	652 ± 15
2.9 ± 0.03	46 ± 2	3716 ± 87	1.22 ± 0.05	53%	NA- 1 hour	75%	845 ± 44
3.0 ± 0.04	40 ± 2	3633 ± 81	1.26 ± 0.07	54%	NA- 4 hours	81%	798 ± 54
3.1 ± 0.02	44 ± 2	3680 ± 77	1.32 ± 0.04	52%	NA- 1 hour	82%	779 ± 27

4.5.2. Fouling characteristics

Understanding where fouling starts in the pan can be used to better mitigate it by focusing on how to minimize fouling in that region. Figure 4.3 shows a test (2.3 g/s inlet flowrate) where fouling occurred at the location shown by the red dot. Fouling started to appear at 13 minutes and at 89 mm from the discharge (Figure 4.3B) and had blocked the flow from reaching the discharge by 15 minutes when the fouling occupied the last 280 mm of the flow path (Figure 4.3C). While 15 minutes was considered the point of failure for the system, Figures 4.3D and 4.3E show what happens if there is no change in the system and no fouling mitigation technique is implemented. These pictures show that fouling occurs near the discharge of the system (this was true for all flow rates where fouling occurred) and continues to build up occupying the flow path moving to the left in the figure (opposite the solution's flow) regardless of the turbulence from boiling, which reduces the evaporation rate.

Fouling first appears near the discharge as it has the maximum amount of water evaporated and therefore the highest salinity, which drives fouling. The last row also has minimal agitation and turbulence as there is minimal boiling due to heater placement. The heater's edges sit 13 mm away from the pan's edge so there is only a small amount of heat applied to the last column and therefore minimal heat is available to continue the boiling. This was done to reduce over evaporating the saline mixture as it exited the system near the discharge and to ensure the heaters were completely covered by the area in the pan where the saline water would travel to avoid heat loss or overheating creating dry-outs.

Boiling locations in the pan are extremely important as boiling increases local shear stress and moves suspended salts in the system as water is evaporated. Where there is no boiling, flow is more stagnant. Salts do not adhere on surfaces where boiling is occurring until significant fouling has occurred because the stress of boiling initially removes any salts that begin to adhere to the aluminum surface. In Figures 4.3C and 3D, salts can no longer be moved to the discharge to exit the system and turbulence from boiling can no longer move them downstream. Therefore, they accumulate and any water in that location will evaporate leaving behind salt particles with high adhesion requiring maintenance to remove them. Before all of the water is evaporated in Figures 4.3B and 4.3C, near the discharge salts are very loose and have low surface adhesion. These salts could easily be dissolved to unblock the flow, or removed with the correct fouling mitigation technique, such as flushing the last column before too much fouling accumulates and impacts system performance.

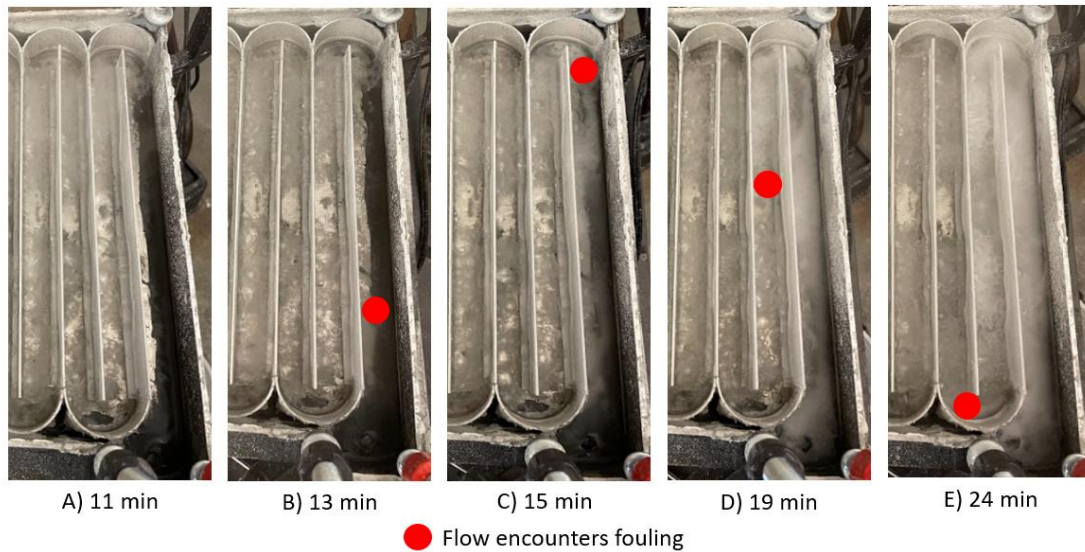


Figure 4.3: Fouling location at A) 11, B) 13, C) 15, D) 19, and E) 24 minutes during a 2.3 g/s inlet flow rate test

4.5.3. Flushing

While tests with less than 52% water evaporation rate were found to be sustainable for several hours, additional measures for mitigating fouling were investigated to be used if it did occur. As previously discussed, fouling begins to accumulate at the last column of the system near the discharge and builds in the direction opposite to the flow direction due to stagnation (reduced boiling) and increased salinity near the discharge. Therefore, attention was focused on identifying a potential fouling mitigation strategy for the last column. Flushing is used in many desalination systems, particularly membrane desalination where air or water applied in the direction opposite of saline mixture flow is used to remove fouling and increase turbulence and shear stress, which has been shown to be effective and sustainable [4]. A 6 mm tube was installed at a 45° angle (see Figure 4.1B) to allow for pure water to be pumped directly into the last column when fouling occurred to remove accumulated salts before they reduced the evaporation rate or efficiency of the system. The inlet was angled to allow flushing the last turn as well, if necessary, and provide flushing over the whole last column. The tube was positioned to only flush the last column to reduce both time and water mass required to flush salts out of the discharge and allowed the rest of the pan to continue evaporating and operating normally. Duration and flow rate of flushing are very important as higher flow rates help push salts out of the way creating a path to the discharge and increase

agitation allowing salts to dissolve quicker. Figure 4.4 shows how a 4.6 g/s flush for 24-seconds removed almost all accumulated salts as pointed out by the dashed boxes. The fouling in the two pictures appears cloudy and the smooth shiny sections of the picture show a clean unfouled pan. In the left picture, before the flush, fouling is dense, and the pan cannot be seen beneath it. However, the right picture, after the flush, shows minimal fouling where single salt crystals can be seen on the pan's surface with a few small cloudier spots showing some accumulated salts (as pointed out by the arrows) but most of the aluminum pan can be seen (uncloudy, shiny surface). Salts that were not removed after the flush are still loose and not attached to the side and could be removed if flush duration was increased, velocity was higher, or applied angle was more direct.

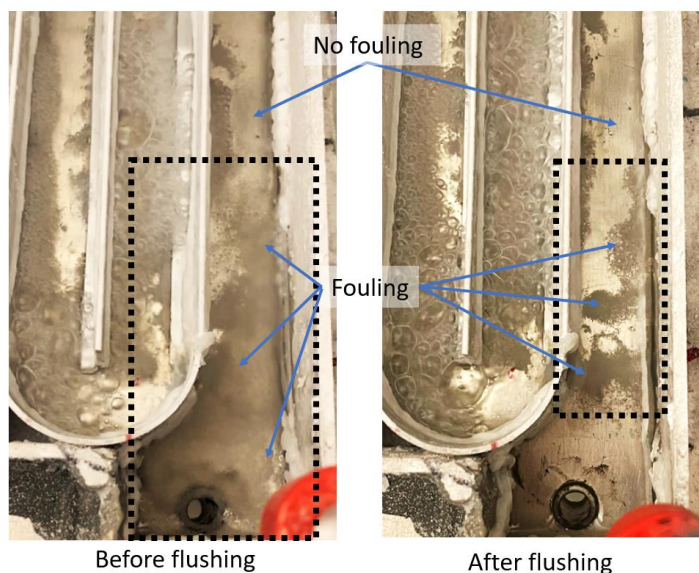


Figure 4.4: Floating pockets of salt in the aluminum pan before (left) and after (right) a 24-second flush at 4.6 g/s

Future work should be done to optimize duration, cycle time, angle, and flow rate of flushing required during testing for different evaporation rates. Flushing could also be performed by a control system as a preventative measure to flush periodically thereby reducing maintenance during operation even when utilizing a water evaporation rate less than 52%.

4.6. Conclusion

An aluminum pan was electrically heated from the bottom to partially evaporate a saline mixture of 10% sodium chloride and 10% potassium chloride in a controlled flow path. This

study demonstrated that controlling flow rates and power could allow a system to be optimized to avoid fouling. By estimating the location of fouling in a system using a model, fouling mitigation techniques could be utilized in a targeted area to minimize disturbance to the overall system and maintain evaporation rates.

- For a saline mixture of 10% sodium chloride and 10% potassium chloride, evaporation greater than 54% results in fouling within the first 30 minutes of testing
- At water evaporation rates higher than 54%, fouling did occur at 295 cm into the flow path and began to accumulate quickly (with 10 minutes) to cover 61 cm of the pan with crystallization fouling as it built in the reverse direction to the flow path and blocked the discharge. Fouling occurred where it was extremely saline and there was minimal boiling, which led to a reduction in turbulence and shear stress needed to help mitigate fouling.
- Targeted flushing was utilized to remove crystallization fouling that occurred near the discharge of the pan by utilizing a port that only flushed that last channel for a brief period. This removed most of the salts and had no effect on the overall evaporation rate of the system as the overall disturbance was minimal.

Future work should be done to optimize duration and cycle time required to flush the system. This will ensure that the system operates as necessary. Flushing should not utilize more than the amount of water evaporated. Further testing should also be done to understand how other parameters, such as temperature and changing velocity by adjusting baffle locations, will affect overall system performance and efficiency.

Declaration of competing interest

The authors declare that they have no known competing financial interests or personal relationships that could have appeared to influence the work reported in this paper.

Acknowledgements

This work is supported by the US Department of Energy, Advanced Research Projects Agency – Energy (ARPA-E) award number DE-AR-0001000. Results of this work do not necessarily reflect the views of the Department of Energy.

Author contributions

Morgan Messer prepared the experimental setup and conducted experimental data. Morgan Messer and Katerina Reynolds analyzed and processed data. Morgan Messer and Bahman

Abbasi conceived and designed the study. Katerina Reynolds prepared the simulation. All authors formulated the paper, approved the final version of the manuscript, and agree to be held accountable for content therein.

References

- [1] F. Macendonio, E. Drioli, A. A. Gusev, A. Bardow, R. Semiat and M. Kurihara, "Efficient technologies for worldwide clean water supply," *Chemical Engineering and Processing: Process Intensification*, vol. 51, pp. 2-17, 2012.
- [2] D. Rubio, C. López-Galindo, J. F. Casanueva and E. Nebot, "Monitoring and assessment of an industrial antifouling treatment. Seasonal effects and influence of water velocity in an open once-through seawater cooling system," *Applied Thermal Engineering*, vol. 67, no. 1-2, pp. 378-387, 2014.
- [3] M. Messer, K. Anderson, X. Zhang and B. Abbasi, "Effect of Surface Roughness on Mixed Salt Crystallization Fouling in Pool Boiling," *Journal of Heat Transfer*, (submitted – under per review).
- [4] M. Bagheri and S. A. Mirbagheri, "Critical review of fouling mitigation strategies in membrane bioreactors treating water and wastewater," *Bioresource Technology*, vol. 258, pp. 318-334, 2018.
- [5] Janzen and E. Y. Kenig, "Understand and Analysis of Fouling Behavior of Bare-Wire heating Elements in Electric Water Heating," *Heat Exchanger Fouling and Cleaning*, 2019.
- [6] F. Albert, W. Augustin and S. Scholl, "Roughness and constriction effects on heat transfer in crystallization fouling," *Chemical Engineering Science*, vol. 66, pp. 499-509, 2010.
- [7] Helalizadeh, H. Müller-Steinhagen and M. Jamialahmadi, "Mixed salt crystallization fouling," *Chemical Engineering and Processing*, vol. 39, pp. 29-43, 2000.
- [8] P. A. Raghupathi and S. G. Kandikar, "Characterization of Pool Boiling of Seawater and Regulation of Crystallization Fouling by Physical Aberration," *Heat Transfer Engineering*, vol. 38, pp. 1296-1304, 2017.
- [9] J. Berce, M. Zupančič, M. Može and I. Golobič, "A Review of Crystallization Fouling in Heat Exchangers," *Processes*, vol. 9, no. 8, 2021.
- [10] M. Jamialahmadi and H. Müller-Steinhagen, "A New Model for the Effect of Calcium Sulfate Scale Formation on Pool Boiling Heat Transfer," *Journal of Heat Transfer*, vol. 126, pp. 507-517, 2004.
- [11] L. Xia, A. W.-K. Law and A. G. Fane, "Hydrodynamic effects of air sparging on hollow fiber membranes in a bubble column reactor," *Water Research*, vol. 47, pp. 3762-3772, 2013.
- [12] Abbasi, X. Zhang, H. O'Hern and E. Nikooei, *Method and System for Purifying Contaminated Water*, 2020.
- [13] H. O'Hern, E. Nikooei, X. Zhang, C. Hagen, N. AuYeung, D. Tew and B. Abbasi, "Reducing the water intensity of hydraulic fracturing: a review of treatment technologies," *Desalination Water Treatment*, vol. 221, pp. 121-138, 2021.

- [14] J. MacAdam and S. A. Parsons, ""Calcium carbonate scale formation and control," *Reviews in Environmental Science and Bio/Technology*, vol. 3, pp. 129-169, 2004.
- [15] Helalizadeh, H. Müller-Steinhagen and M. Jamialahmadi, "Mathematical modeling of mixed salt precipitation during convective heat transfer and sub-cooled flow boiling," *Chemical Engineering Science*, vol. 60, pp. 5078-5088, 2005.
- [16] Lynn, A. Medved and T. Griggs, "A comparative analysis on the impact of salinity on the heat generation of OTEC plants to determine the most plausible geographical location," *PAM Review*, 2018.
- [17] M. H. Sharqawy and S. M. Zubair, "Thermophysical properties of seawater: A review of existing correlations and data," *Desalination and Water Treatment*, vol. 16, pp. 354-380, April 2010.
- [18] H. Coleman and W.G. Steele, "Engineering Application of Experimental uncertainty Analysis", *AIAA Journal*, vol 33, No. 10, pp 1888-1896, October 1995
- [19] M. Laliberté and W. E. Cooper, "Model for Calculating Density of Aqueous Electrolyte Solutions," *Journal of Chemical Engineering*, vol. 49, pp. 1141-1151, 2004.

CHAPTER 5: Thesis conclusions and future recommendations

5.1. Thesis summary

In **Chapter 1**, an overview of desalination technologies, hydraulic fracking wastewater, and fouling was presented. SCEPTEr (Selective Condensation and Evaporation using Precise Temperature Regulation) was presented as a solution to treating hydraulic fracking wastewater. This thesis focused on the development of a humidification system that will remove less volatile contaminants from a wastewater stream, manage fouling, and be competitive in cost with other technologies. It also presented the thesis objectives: to determine the most applicable humidification method for the SCEPTEr system, to determine the effect of surface roughness in a highly saline mixed salt pool boiling on the fouling resistance and heat transfer coefficient, and design and control an evaporation system to mitigate fouling.

In **Chapter 2**, spray humidification and a venturi mixing nozzle paired with a boiling system were compared to determine their applicability with a highly saline wastewater stream. This chapter addressed the first of the research questions expressed in section 1.5: a comparison between spray evaporation and flow evaporation is needed to access both energy and water quality. Spray humidification was found to consume 20-30% less overall energy but has a high risk of entraining contaminants in the humid air stream that would recontaminate the produced water. The venturi nozzle humidification method was more energy intensive but has a low risk of recontaminating the produced water and is easily controlled by adjusting the power and inlet flow rate. Further testing would need to be done to ensure that the spray humidification system could remove the less volatile contaminants before it could be implemented with contaminants other than dissolved solids (salt) which could be removed with a cyclone.

Chapter 3 addressed the second of the research questions expressed in section 1.5: fouling accumulation must be quantified for various surface roughness'. Experimental testing with 20% saline (concentrated seawater salts) flow boiling environment was utilized to determine the effect of various average surface roughness values (0.35 μm , 5 μm , 10.5 μm microchannel) on the fouling resistance and heat transfer coefficient. To improve the fouling resistance the surface roughness must be very smooth (0.35 μm). If it was still sufficiently

rough (homogeneous 5 μm -10.5 μm microchannel) there was no additional benefit to either the fouling resistance or the heat transfer coefficient. Therefore, to manufacture a semismooth (5 μm) surface may have minimal impact on the overall system but increases costs. In addition, 3% ethylene glycol was added to the saline solution to determine its effect on fouling resistance and the heat transfer coefficient. It had minimal effect on the overall fouling accumulation and resistance but did reduce the amount of sodium salts. Organic compounds such as ethylene glycol could be utilized to target specific salts from forming on the heat exchanger surface.

Chapter 4 addresses the third research question presented in section 1.5 stating that the crystallization fouling in flow evaporation must be characterized and managed during steady state operation. An experimental study was presented with 20% saline (10% NaCl and 10% KCl) in a flow boiling environment to determine the operational point when crystallization fouling reduces system operation and restricts the discharge flow. The inlet flow rate was adjusted from 2.3-3.1 g/s with 3730 W of electrical heating power. For flow rates less than 2.8 g/s fouling occurred in the first 30 minutes of testing and required additional fouling mitigation methods to clear the system such as targeted flushing. For 2.9-3.1 g/s inlet flow rate the water evaporation rate remained steady at 52-54% for 4 hours with no fouling. Therefore, a water evaporation rate of less than 54% could be sustainable for longer periods of time while still evaporating and humidifying a highly saline inlet stream. The fouling accumulation at lower flowrates occurred near the discharge and began to accumulate in the counterflow direction as it blocked the discharge from allowing deposited salts to exit. Flushing was utilized on the last flow path to remove fouling before it adhered to the surface and became more difficult to remove. Flushing had no negative impact on the evaporation rate in the rest of the tank.

5.2. Future recommendations

Future work is needed to generalize the information and data presented in Chapter 4 for other desalination systems and broaden the application of this work. This includes looking at the effect of flow rate, water velocity, and film thickness on the fouling accumulation and suggested operating point. Additional contaminants should be tested in flow and pool boiling environments with high salinity to understand the effect on fouling accumulation and suggested water evaporation operating point to understand both the sensibility and real-world application of this work. Quantifying ions' interactions and the order in which salts

precipitate from the solution will help better understand and mitigate fouling in the SCEPTER system and optimize its control strategy. Future work should quantify different operating parameters based on different salinities and salts as well as optimize the duration and cycle time of the flushing mitigation measure to ensure optimal operation.